JCI The Journal of Clinical Investigation

Neural precursor cell–secreted TGF-β2 redirects inflammatory monocyte-derived cells in CNS autoimmunity

Donatella De Feo, … , Melanie Greter, Gianvito Martino

J Clin Invest. 2017;127(11):3937-3953. https://doi.org/10.1172/JCI92387.

Research Article **Autoimmunity** **Stem cells**

In multiple sclerosis, the pathological interaction between autoreactive Th cells and mononuclear phagocytes in the CNS drives initiation and maintenance of chronic neuroinflammation. Here, we found that intrathecal transplantation of neural stem/precursor cells (NPCs) in mice with experimental autoimmune encephalomyelitis (EAE) impairs the accumulation of inflammatory monocyte-derived cells (MCs) in the CNS, leading to improved clinical outcome. Secretion of IL-23, IL-1, and TNF-α, the cytokines required for terminal differentiation of Th cells, decreased in the CNS of NPC-treated mice, consequently inhibiting the induction of GM-CSF–producing pathogenic Th cells. In vivo and in vitro transcriptome analyses showed that NPC-secreted factors inhibit MC differentiation and activation, favoring the switch toward an antiinflammatory phenotype. *Tgfb2*$^{-/-}$ NPCs transplanted into EAE mice were ineffective in impairing MC accumulation within the CNS and failed to drive clinical improvement. Moreover, intrathecal delivery of TGF-β2 during the effector phase of EAE ameliorated disease severity. Taken together, these observations identify TGF-β2 as the crucial mediator of NPC immunomodulation. This study provides evidence that intrathecally transplanted NPCs interfere with the CNS-restricted inflammation of EAE by reprogramming infiltrating MCs into antiinflammatory myeloid cells via secretion of TGF-β2.

Neural precursor cell–secreted TGF-β2 redirects inflammatory monocyte-derived cells in CNS autoimmunity

Donatella De Feo,[1,2] Arianna Merlini,[1,2] Elena Brambilla,[1] Linda Ottoboni,[1] Cecilia Laterza,[1] Ramesh Menon,[3] Sundararajan Srinivasan,[3] Cinthia Farina,[3] Jose Manuel Garcia Manteiga,[4] Erica Butti,[1] Marco Bacigaluppi,[1,2] Giancarlo Comi,[2] Melanie Greter,[5] and Gianvito Martino[1]

[1]Neuroimmunology Unit, [2]Department of Neurology, [3]Immunobiology of Neurological Disorders Lab, Institute of Experimental Neurology, Division of Neuroscience, and [4]Center for Translational Genomics and BioInformatics, San Raffaele Scientific Institute and Vita Salute San Raffaele University, Milan, Italy. [5]Institute of Experimental Immunology, University of Zürich, Zürich, Switzerland.

In multiple sclerosis, the pathological interaction between autoreactive Th cells and mononuclear phagocytes in the CNS drives initiation and maintenance of chronic neuroinflammation. Here, we found that intrathecal transplantation of neural stem/precursor cells (NPCs) in mice with experimental autoimmune encephalomyelitis (EAE) impairs the accumulation of inflammatory monocyte-derived cells (MCs) in the CNS, leading to improved clinical outcome. Secretion of IL-23, IL-1, and TNF-α, the cytokines required for terminal differentiation of Th cells, decreased in the CNS of NPC-treated mice, consequently inhibiting the induction of GM-CSF–producing pathogenic Th cells. In vivo and in vitro transcriptome analyses showed that NPC-secreted factors inhibit MC differentiation and activation, favoring the switch toward an antiinflammatory phenotype. *Tgfb2*$^{-/-}$ NPCs transplanted into EAE mice were ineffective in impairing MC accumulation within the CNS and failed to drive clinical improvement. Moreover, intrathecal delivery of TGF-β2 during the effector phase of EAE ameliorated disease severity. Taken together, these observations identify TGF-β2 as the crucial mediator of NPC immunomodulation. This study provides evidence that intrathecally transplanted NPCs interfere with the CNS-restricted inflammation of EAE by reprogramming infiltrating MCs into antiinflammatory myeloid cells via secretion of TGF-β2.

Introduction

Multiple sclerosis (MS) is an autoimmune disease of the central nervous system (CNS), representing the most common CNS inflammatory disorder and the second leading cause of disability in young adults. In experimental autoimmune encephalomyelitis (EAE), the animal model of MS, myelin-reactive pathogenic T helper (Th) cells enter the CNS at the level of pial vessels and are reactivated in the subarachnoid space by meningeal perivascular macrophages (1) that allow pathogenic Th cells tissue entry and initiation of inflammation (2). Pathogenic Th cells induce, through granulocyte-macrophage colony-stimulating factor (GM-CSF), an inflammatory program in monocytes and their progeny, monocyte-derived dendritic cells (moDCs) (2, 3). In the CNS, moDCs function as antigen-presenting cells (APCs) to pathogenic Th cells, secreting polarizing cytokines such as IL-1, IL-23, IL-6, and TNF-α (4–7), and directly contribute to myelin and axonal loss via phagocytosis and the production of ROS and other neurotoxic mediators (3, 8).

Although available therapies for MS effectively target the recruitment of T cells from the periphery into the CNS (9), there is no conclusive evidence regarding their ability to target either the self-maintaining inflammatory cycle that occurs locally within the CNS or the pathogenic phenotype of CNS-infiltrating monocyte-derived cells (MCs) (10).

Neural precursor cells (NPCs) have been previously studied as a therapeutic strategy for MS for their regenerative potential, and, more recently, for their neuroprotective and immunomodulatory properties (11–14). NPCs express chemokine receptors and adhesion molecules that allow them, upon transplantation, to reach inflamed areas in the CNS (11, 15–17) and to release a variety of cytokines and neurotrophins that can inhibit the adaptive and innate immunity (18–20). While previous studies found intrathecal transplantation of NPCs to ameliorate EAE disease severity (14, 21, 22), the immunological mechanism underlying the therapeutic efficacy of NPCs delivered in the inflamed CNS still remains unknown.

In this work we investigated whether intrathecal NPC treatment could directly interfere with the CNS-restricted crosstalk between pathogenic Th cells and inflammatory MCs. We found that NPC treatment impaired the accumulation of infiltrating MCs in the CNS and reduced EAE disability. In fact, NPCs limited the expression of cytokines required for the polarization of encephalitogenic GM-CSF–producing Th cells. NPCs inhibited in vivo and in vitro DC differentiation and maturation, favoring a fate switch toward an antiinflammatory phenotype. We identified TGF-β2 as the primary factor secreted by NPCs for the observed therapeutic effect in the chronic phase of EAE.

Conflict of interest: The authors have declared that no conflict of interest exists.
Submitted: January 5, 2017; **Accepted:** August 2, 2017.
Reference information: *J Clin Invest*. 2017;127(11):3937–3953.
https://doi.org/10.1172/JCI92387.

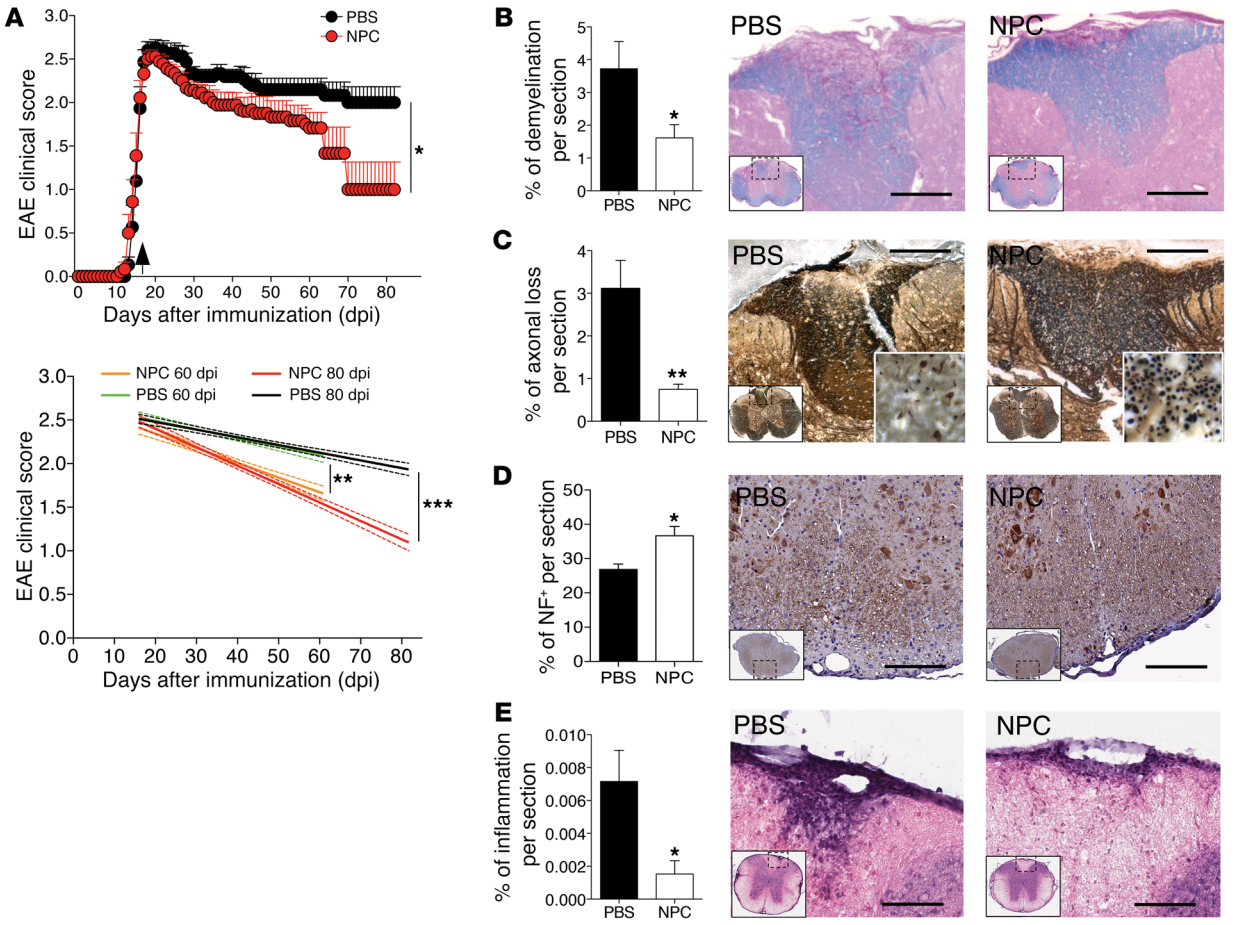

Figure 1. Intrathecally administered NPCs ameliorate chronic EAE. (**A**) Top: Clinical scores of EAE mice treated at the peak of the disease (4 days after the clinical onset, arrow) with intrathecal injection (into cisterna magna) of either NPCs (red dots) or PBS (black dots), n = 20 mice per group. Each point represents the mean ± SEM; 70 to 82 dpi, 2-way ANOVA with Bonferroni's post-test, $^{*}P \le 0.05$. Bottom: Linear regression curves of clinical score from the day of treatment with either NPCs or PBS until 60 or 80 dpi. Dashed lines indicate 95% CI. $^{**}P \le 0.01$; $^{***}P \le 0.001$. (**B**–**D**) Quantification and representative images of spinal cord demyelination (Luxol fast blue staining) (**B**) and axonal loss quantified on Bielschowsky silver staining (**C**; at bottom right, high-magnification insets, ×100) and immunohistochemistry for neurofilaments (NF) (**D**) at 80 dpi in PBS-treated (black bars) versus NPC-treated (white bars) EAE mice (n = 15 sections per mouse, 3–6 mice per group). (**E**) Quantification and representative images of inflammatory infiltrates (H&E staining) at 30 dpi in PBS-treated (black bars) versus NPC-treated (white bars) EAE mice (n = 12–20 sections per mouse, 3 mice per group). Data are mean ± SEM and represent the percentage area of damage over total section area. $^{*}P \le 0.05$, $^{**}P \le 0.01$, unpaired t test. Scale bars: **B**–**E**, 100 μm.

Results

Intrathecal NPC transplantation ameliorates EAE by reducing inflammatory MCs in the CNS. To examine the capacity of NPC transplantation to inhibit the CNS-restricted inflammation occurring in EAE, we first validated the therapeutic potential of intrathecal NPC injection in C57BL/6 mice immunized with myelin oligodendrocyte glycoprotein $(MOG)_{35-55}$ peptide. One million NPCs in PBS (NPC-treated) or PBS alone (PBS-treated) was intrathecally injected into the cisterna magna at the peak of disease severity, 4 days after clinical onset. We observed that NPC-treated mice displayed faster recovery and lower disability compared with EAE mice treated only with PBS (Figure 1A). At 1 month after treatment (60 days postimmunization [dpi]), NPC-treated mice showed significantly lower neurological impairment, and at the end of the follow-up (80 dpi), NPC-treated mice showed either complete functional recovery or minor tail paralysis, while PBS-treated mice maintained an overt paresis of the hind limbs. Accordingly, NPC-treated mice displayed a lower lesion burden measured as demyelination and axonal loss in the spinal cord at the end of follow-up (Figure 1, B–D). Interestingly, we found 2 weeks after treatment (40 dpi) a significant reduction of the inflammatory infiltrate areas (Figure 1E) and in particular of $CD3^+$ T cells (Supplemental Figure 1A; supplemental material available online with this article; https://doi.org/10.1172/JCI92387DS1) and of $IB4^+$ phagocytes (Supplemental Figure 1B) in the spinal cord of NPC-treated compared with PBS-treated mice. We further observed that NPC-treated mice, compared with PBS-treated controls, already at this early time point, displayed a parallel reduction of both inflammation ($IBA1^+$ areas) and demyelination (loss of MBP^+ areas) in the spinal cord (Supplemental Figure 1, C and D). At this same time point, we observed that most transplanted GFP^+ NPCs localized in the subarachnoid space of cerebellum, brainstem, and cervical spinal cord, with similar spatial distribution of infiltrating extraparenchymal $CD11b^+$ myeloid cells (Figure 2, A and B, and Supplemental Figure 2A). Transplanted NPCs were found in proximity to meningeal vessels and $CD45^+$ perivascular inflammatory cells,

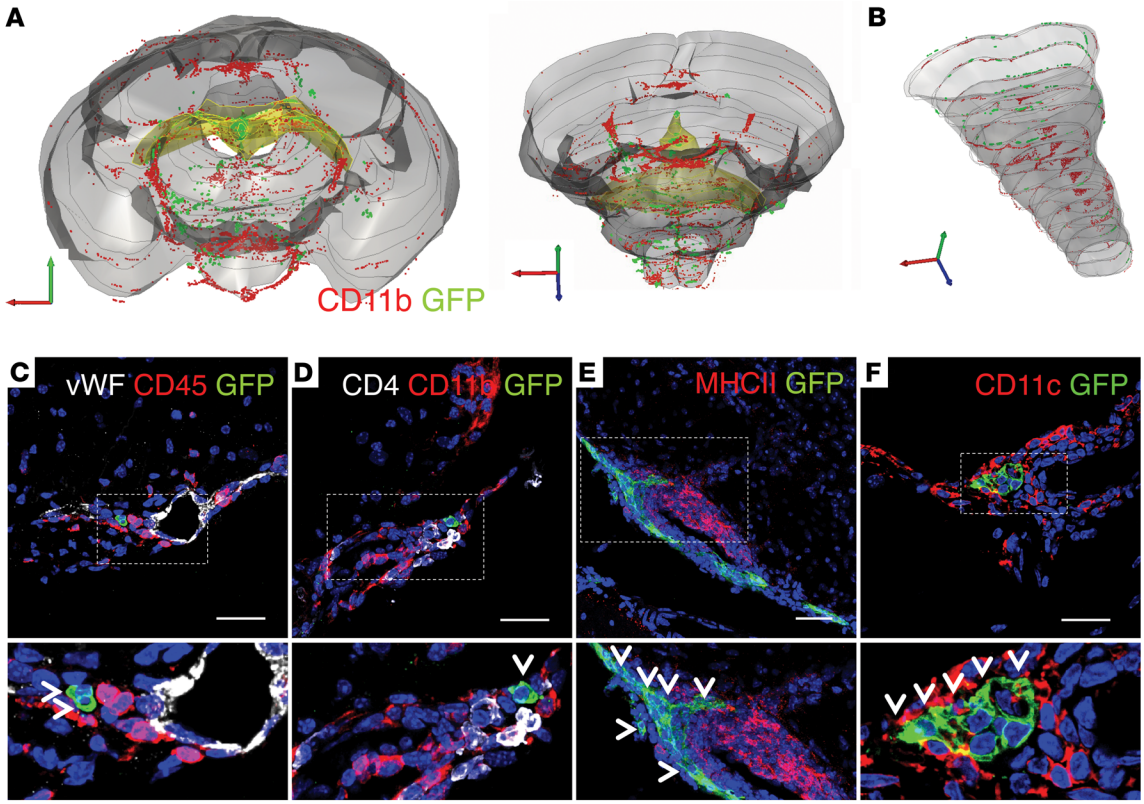

Figure 2. Transplanted NPCs distribute in the subarachnoid space within the inflammatory infiltrates. (**A** and **B**) Representative 3D reconstruction of the relative distribution of transplanted NPCs (GFP$^+$ in green) and CD11b$^+$ inflammatory cells (in red) within the hindbrain (**A**, rostral and caudal view) and the cervical spinal cord (**B**) (outlined in gray), the cerebral aqueduct and IV ventricle (outlined in yellow), in an NPC-treated mouse at 7 days after transplantation, obtained from a total of n = 33 sequential stereology sections. (**C**–**F**) Representative immunofluorescence images of intrathecally transplanted NPCs (GFP$^+$ in green, arrowheads in the magnified insets, shown below, of the above dashed boxes) that localize in the meningeal perivascular spaces of the spinal cord and brainstem, often detected in proximity to von Willebrand factor–positive (vWF$^+$) endothelial cells (white in **C**), to CD45$^+$ blood-derived leukocytes (red in **C**), to perivascular infiltrating CD11b$^+$ myeloid cells (red in **D**), to CD4$^+$ T cells (white in **D**), and to MHC-II$^+$ as well as CD11c$^+$ local APCs (red in **E** and **F**, respectively). Nuclei are stained by DAPI (blue). Scale bars: **C**–**F**, 25 μm.

including CD4$^+$ T cells, CD11b$^+$ myeloid cells, MHC class II$^+$ cells, and CD11c$^+$ DCs (Figure 2, C–F). Transplanted NPCs retained an undifferentiated phenotype up to the end of follow-up, at 80 dpi, displaying only in low percentage markers for neuronal (β-tubulin III, β-tub III$^+$), oligodendroglial (oligodendrocyte lineage transcription factor 2, Olig2$^+$), or astroglial lineage (glial fibrillary acidic protein, GFAP$^+$) (Supplemental Figure 2, B–D and G). Further, transplanted NPCs expressed the stem cell marker nestin and the proliferation marker Ki-67 (Supplemental Figure 2, E and F). Notably, intrathecally transplanted GFP$^+$ NPCs were detected only in the CNS of NPC-transplanted mice (Supplemental Figure 3, A and B), while NPCs were found neither in peripheral organs (Supplemental Figure 3, C–E) nor in secondary lymphoid organs (Supplemental Figure 3, F–H).

To better investigate the mechanism regulating the clinical and pathological recovery induced by transplanted NPCs, we performed flow cytometry analysis of CNS-resident and infiltrating inflammatory cells of EAE mice 7 days after NPC or PBS treatment. We observed a significant reduction in frequency and cell number of inflammatory MCs (CD45^{hi}CD11b$^+$Ly6G$^-$Ly6C$^+$CD11c$^+$MHC-II$^+$) (23) as well as a trend of reduction of infiltrating lymphoid cells (CD45^{hi}CD11b$^-$) in the CNS of NPC-treated compared with PBS-treated EAE mice (Figure 3, A–C). Microglia (CD45^{lo}CD11b$^+$Ly6G$^-$Ly6C$^-$) were not quantitatively altered after NPC treatment (Figure 3, A and D), but displayed lower expression of MHC-II (Figure 3, E and F), suggestive of a lower activation state.

NPC treatment hampers the effector phase of EAE. The accumulation of myeloid cells in the CNS during the effector phase of EAE relies on the ability of CNS-invading Th cells to secrete GM-CSF (2, 3). NPC-transplanted mice had significantly lower frequencies of GM-CSF$^+$ cells in CNS-infiltrating Th1 and Th17 cells (Figure 4A) as well as in total CD4$^+$ T cells (Figure 4B). No significant difference between NPC- and PBS-treated mice, neither in the frequency of FoxP3$^+$ Tregs nor in the level of FoxP3 expression by CNS-infiltrating CD4$^+$ T cells, was observed (Figure 4, C and D). Consistently, CD4$^+$ T cells in the CNS showed significantly lower expression of transcripts related to Th17 pathogenicity (24), such as *Il23r*, *Rorc*, *Tbx21*, *Il22*, *Cxcl3*, and *Csf2*, in NPC-treated mice (Figure 4E). Furthermore, GM-CSF levels were significantly reduced in the hindbrain and cervical spinal cord of NPC-treated mice (Figure 4F).

The capacity of autoreactive Th cells to secrete GM-CSF depends on the production of proinflammatory cytokines by moDCs (2, 3, 7, 25). Seven days after transplantation, we found

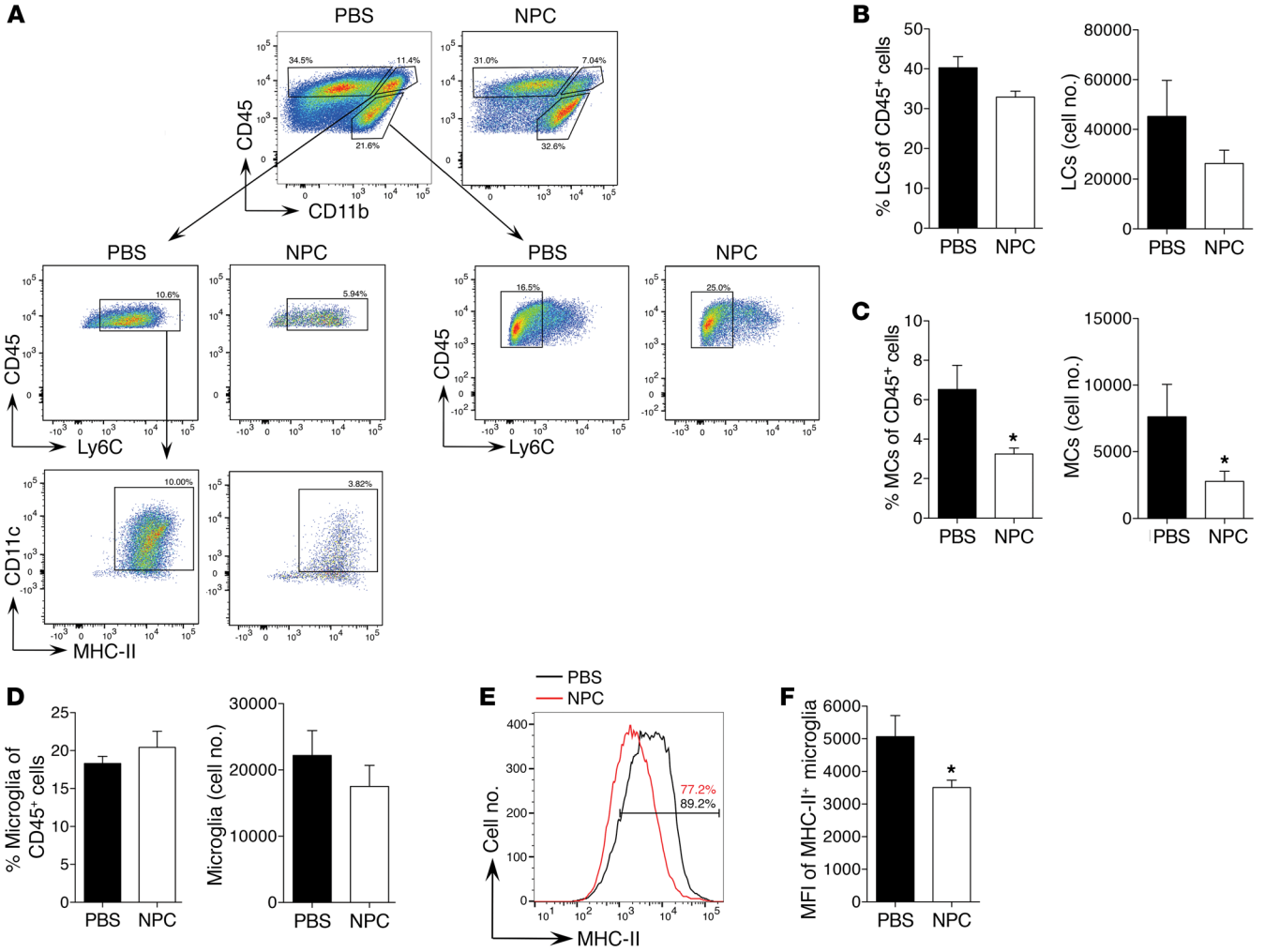

Figure 3. NPC transplantation reduces the accumulation of inflammatory MCs and the activation of microglia during the effector phase of EAE. (**A**–**D**) Flow cytometry of CNS leukocytes from PBS- and NPC-treated EAE mice, assessed at day 7 after transplantation. Frequencies and total cell number of CNS-infiltrating lymphoid cells (LCs; $CD45^{hi}CD11b^{+}$) and inflammatory MCs ($CD45^{hi}CD11b^{+}Ly6G^{-}Ly6C^{hi}CD11c^{+}MHC\text{-}II^{+}$) are shown in the plots (**A**) and quantified in the graphs (n = 4–5 mice per group) (**B** and **C**). Frequencies and total cell number of CNS-resident microglia ($CD45^{int}CD11b^{+}Ly6G^{-}Ly6C^{-}$) are shown in the plots (**A**) and quantified in the graphs (n = 4–5 mice per group) (**D**). (**E** and **F**) Level of MHC-II on microglia in PBS-treated (black line) and NPC-treated EAE mice (red line) at day 7 after transplantation is shown in the histogram (mean fluorescence intensity, MFI) (**E**) and quantified in the graph (n = 4 mice per group) (**F**). Black bars, PBS-treated mice; white bars, NPC-treated mice. Data are mean ± SEM and are representative of 2 independent experiments. *$P \leq 0.05$, unpaired t test.

significantly lower expression of *Il23a* and *Tnfa* transcripts in the CNS inflammatory infiltrate of NPC-treated mice (Figure 5A). Moreover, IL23p19 protein levels were significantly reduced in the CNS of NPC-transplanted mice (Figure 5B). Accordingly, cytokine profiling of CNS tissues revealed also decreased levels of IL-1β and TNF-α and of IL-23–related factors such as G-CSF, CXCL1, and IL-17A (Figure 5C). These findings support the idea that NPC treatment dampens the production of polarizing cytokines by inflammatory MCs, which in turn reduce GM-CSF production and the pathogenic potential of CNS-invading Th cells.

NPC-secreted factors inhibit maturation of DCs and their capacity to trigger GM-CSF production in myelin-reactive Th cells. We hypothesized that an NPC-secreted factor could inhibit the antigen-presenting and proinflammatory properties of myeloid cells. To investigate this hypothesis, we exposed in vitro bone marrow–derived DCs (BMDCs) to NPC-conditioned medium (NCM) or control DC culture medium (DCM) during stimulation with CD40L, mimicking T cell interaction with APCs. BMDCs exposed to NCM expressed lower levels of MHC-II and of the costimulatory molecules CD80 and CD86 compared with BMDCs in DCM (Figure 6, A and D). Cytokine profiling showed that BMDCs exposed to NCM produced a significantly lower amount of polarizing cytokines, including TNF-α, IL23p19, IL-6, and IL12p70 and chemokines such as CXCL10, CXCL1, and G-CSF (Figure 6B). We further confirmed the inhibitory effect of NCM on IL-23 and TNF-α production by ELISA (Figure 6C) and quantitative PCR (Figure 6D). Finally, we assessed the ability of BMDCs exposed to NCM during CD40L stimulation to reactivate $CD4^{+}$ T cells from MOG_{35-55} peptide–immunized 2D2 mice. Conditioning of BMDCs with NCM during CD40L stimulation decreased their ability to induce the production of GM-CSF in Th1 and Th17 cells (Figure 7).

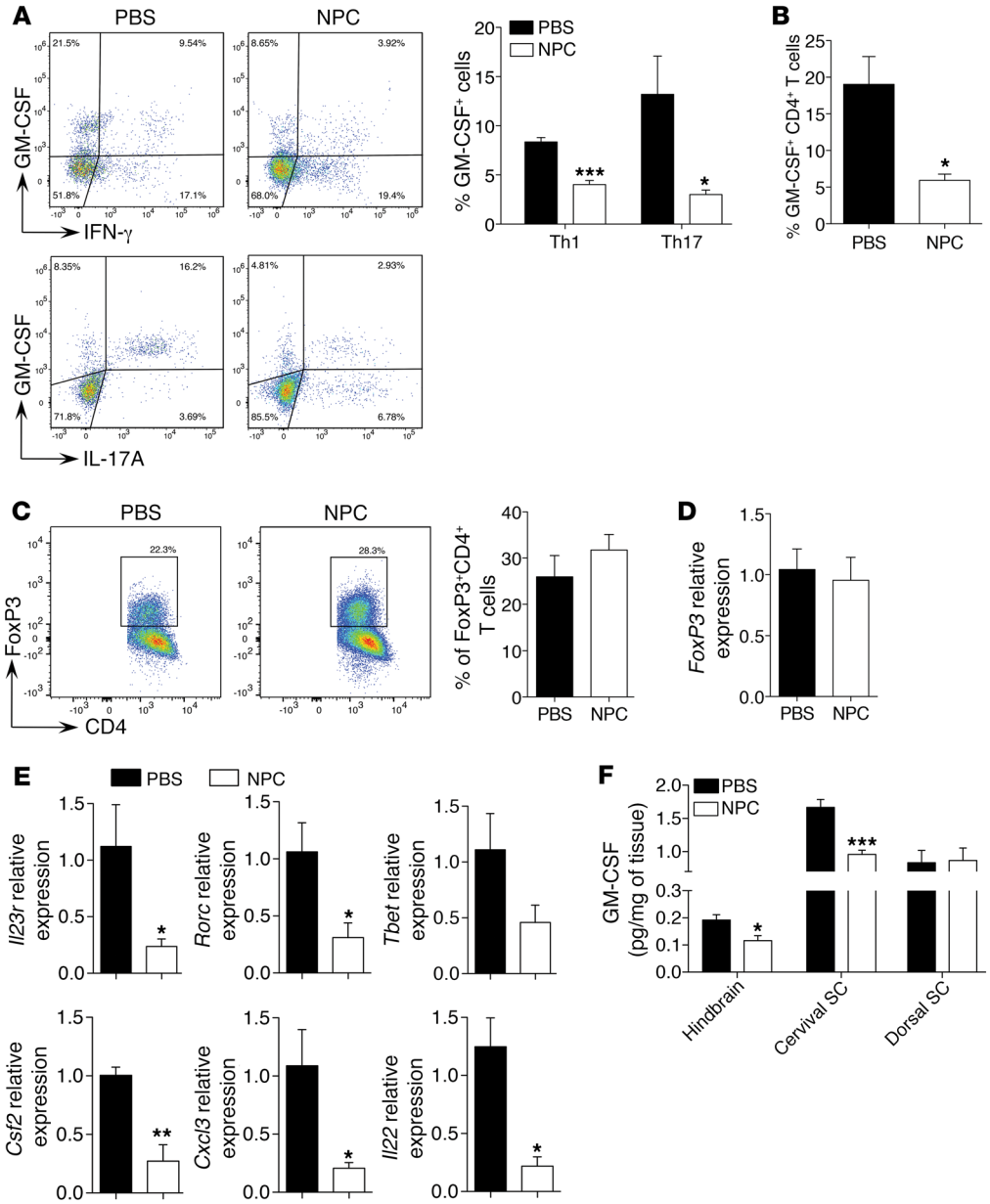

Figure 4. NPC transplantation dampens the pathogenic signature of the CNS-infiltrating Th cells. (**A** and **B**) Production of GM-CSF by CNS-infiltrating Th1 ($CD45^{hi}CD3^{+}CD4^{+}IFN\text{-}\gamma^{+}$) and Th17 cells ($CD45^{hi}CD3^{+}CD4^{+}IL\text{-}17A^{+}$) in EAE mice 7 days after PBS or NPC treatment as analyzed by flow cytometry. Frequency of $GM\text{-}CSF^{+}$ Th1, $GM\text{-}CSF^{+}$ Th17, and total $GM\text{-}CSF^{+}$ Th cells are shown in the plots (**A**) and quantified in the graph (n = 4 mice per group) (**B**). (**C**) Frequency of $FoxP3^{+}$ CNS-infiltrating $CD4^{+}$ T cells ($CD45^{hi}CD11b^{-}CD4^{+}$) in PBS- and NPC-treated EAE mice at the same time point as **A** is shown in plots and graph (n = 4 mice per group). (**D** and **E**) Expression of *FoxP3* (**D**) and *Rorc*, *Il23r*, *Tbet*, *Il22*, *Csf2*, and *Cxcl3* (**E**) in $CD45^{hi}CD11b^{-}CD4^{+}$ Th cells sorted from the CNS of PBS- and NPC-treated EAE mice at the same time point, relative value to PBS-treated mice (n = 4 mice per group). (**F**) GM-CSF quantification by ELISA in hindbrain and cervical and dorsal spinal cord (SC) tissues of PBS- and NPC-treated EAE mice at 7 days after transplantation (n = 6 mice per group). Black bars, PBS-treated mice; white bars, NPC-treated mice. Data are mean ± SEM and are representative of 2 independent experiments. $^{*}P \le 0.05$, $^{**}P \le 0.01$, $^{***}P \le 0.001$, unpaired t test.

In conclusion, NPC-secreted factors inhibit in vitro the capacity of DCs to induce GM-CSF–producing pathogenic Th cells.

NPC-secreted factors guide transcriptional reprogramming of inflammatory DCs toward an alternative antiinflammatory activation. We next sought to dissect the sequence of molecular events triggered by NPCs that induces immunomodulation in inflammatory myeloid cells. To follow over time the dynamic changes induced by NPCs in BMDCs, we performed gene expression profiling on BMDCs after 6 and 18 hours of CD40L stimulation in the absence (mDC) or presence of NCM (mDC-NCM). WT unstimulated immature DCs (iDCs) were used as reference group to identify maturation-related transcripts (Figure 8A).

Bioinformatics analysis identified 2 sets of unique genes that were differentially regulated between mDC and mDC-NCM after 6 or 18 hours in culture with a significance threshold of $P \le 0.01$ (Figure 8A and Supplemental Table 1).

Unsupervised hierarchical clustering clearly separated NCM-treated mDC from control mDC, both at the early (6 hours) and at the late (18 hours) time point (Figure 8B). Subclustering analysis at each time point highlighted subsets of genes shared only between mDC-NCM and iDCs, suggesting an impairment of the CD40L-induced maturation by NPC-secreted factors (Figure 8B). However, the exposure to NCM during CD40L stimulation instructed in DCs a specific gene expression signature, demonstrating the induction of an alternative program of activation/differentiation.

Indeed, gene ontology analysis identified enriched functional groups associated with metabolic processes (*Arg1*, *Arg2*, ferroportin-1), macromolecule biosynthesis, regulation of transcription (*Cbx5* and *Itch*), and programmed cell death in mDC-NCM at the early time point (Figure 8C). Genes related to oxidative stress and apoptosis resistance, such as *Ak2*, *Tgm2*, and *Smarca2* (26, 27), were upregulated whereas proapoptotic genes such as

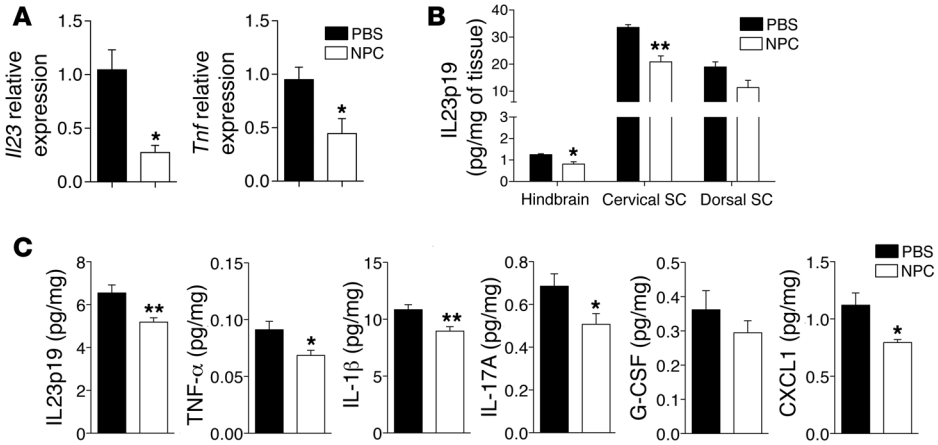

Figure 5. NPC transplantation impairs the production of polarizing cytokines by CNS-infiltrating APCs. (**A**) Expression of *Il23* and *Tnf* in CNS leukocytes isolated from EAE mice at 7 days after PBS or NPC treatment, relative value to PBS-treated mice (n = 3 mice per group). Data are representative of 2 independent experiments. (**B**) ELISA for IL23p19 in hindbrain and cervical and dorsal spinal cord tissues from PBS- and NPC-treated EAE mice obtained at the same time point as **A** (n = 3 mice per group). Data are representative of 2 independent experiments. (**C**) Cytokine profile in hindbrain tissues of PBS- and NPC-treated mice obtained at the same time point as **A**. Hindbrain tissue lysates were analyzed for expression of various cytokines by Luminex-based assay (n = 10 mice per group). Black bars, PBS-treated; white bars, NPC-treated. Data are mean ± SEM. $^*P \le 0.05$, $^{**}P \le 0.01$, unpaired t test.

Tnfrsf6 (Fas) were downregulated in mDC-NCM. In addition, NCM induced in DCs transcripts related to the alternative or antiinflammatory phenotype, such as *Arg1*, *Maf*, *Itch*, *Stab1*, and *Tgm2* (28–32). Accordingly, mDC-NCM also upregulated the expression of *Ddx21*, which is required for the induction of *S100A9* (33), an immaturity marker of myeloid-derived suppressor cells (MDSCs) (ref. 34; Figure 8, B and E; and Supplemental Table 1). At 18 hours, gene ontology analysis of NCM-regulated genes confirmed the NCM-induced shift of mDC toward an antiinflammatory activation. Indeed, NCM-treated mDC had a significantly lower expression of genes encoding proinflammatory chemokines (*Ccl1*, *Ccl2*, *Ccl3*, *Ccl7*, *Ccl8*, *Cxcl2*) (3, 35), positive regulators of cytokine production (*CD36*, *Il33*, *Clec9a*, and *Clec5a*) (36–39), and phagocytosis-related genes (*Ptx3*, *Elmo2*, *Clec7a*) (ref. 3 and Figure 8, B, D, and F). Conversely, NCM induced the antiinflammatory molecules *Hspa1a*, which impairs the stimulatory capacity of moDCs (40), and *Il1r2*, the IL-1 decoy receptor that blocks IL-1 signaling in inflammatory macrophages (41) and the NF-κB inhibitor *Ascc1* (ref. 42; Figure 8, B, D, and F; and Supplemental Table 1).

Transcription factor analysis of early (6 hours) NCM-regulated genes showed an enrichment in positively regulated transcripts controlled by c-Myc, a master regulator in macrophage alternative activation (43, 44), and c/EBPβ, which is the main regulator of MDSC differentiation (ref. 45 and Supplemental Figure 4A). At the later time point (18 hours), many negatively NCM-regulated transcripts were enriched in genes controlled by PU.1 (46) and NF-κB1, both pivotal in DC differentiation and maturation (Supplemental Figure 4B, Supplemental Table 2, and refs. 46, 47).

When we compared the differentially expressed genes of CD40L-induced maturation in the absence (iDCs vs. mDC) or presence of NCM (iDCs vs. mDC-NCM), we identified pathways only modulated during the maturation induced in the presence of NPC-secreted factors. The pathways included at 6 hours the antiapoptotic TNFs/NF-κB/BCL-2 pathway and NFAT in immune response (Supplemental Figure 5A), and at 18 hours IL-4–induced regulators, p53 signaling, NO synthesis and signaling, Fas signaling, and TGF-β–dependent activation, and were associated with an alternative activation of DCs (Supplemental Figure 5B).

Specifically, among early NCM-regulated genes, *Rad51* (48) and *Arhgap15* (49), known to be inhibited by TGF-β, were downregulated, while *Arg1*, which is induced by TGF-β (ref. 50; Figure 8, A and E; and Supplemental Table 1), was increased. Similarly, *CD36* and *Il33*, both inhibited by TGF-β, were significantly downregulated in mDC-NCM at 18 hours (ref. 51; Figure 8, B, D, and F; and Supplemental Table 1).

We therefore investigated whether NPCs could influence myeloid cell differentiation and activation also in vivo and possibly through TGF-β signaling during EAE. To this end, $MOG_{35–55}$-immunized EAE mice were injected, at the peak of the disease, with 10^6 NPCs or vehicle. At 7 days after transplantation, CNS-infiltrating MCs were FACS-sorted (Figure 9A) and mRNA was extracted. Next-generation sequencing was performed, and genome-wide profiles were generated and compared between MCs isolated from the CNS of NPC-treated animals and PBS-treated animals in EAE. We identified 610 genes that were differentially expressed with the significance threshold of $P \le 0.01$ (Figure 9B and Supplemental Table 3). Hallmark gene set enrichment analysis confirmed the modulation of metabolic processes and of several immunological pathways, including TGF-β signaling, the IFN response, and genes upregulated by ROS, in MCs from NPC-treated mice (Figure 9, C and D). In line with in vitro data, transcription factor analysis found c-Myc and CREB1 (Supplemental Figure 6 and Supplemental Table 4), master transcription factors for the alternative activation of macrophages (43, 52), as main regulators of NPC-induced gene signature in CNS-infiltrating MCs.

Overall these findings suggest that NPC-secreted factors skew the inflammatory differentiation program of MCs toward an alternative/antiinflammatory activation (53), possibly through TGF-β signaling, both in vitro, during DC activation, and in vivo, in the inflamed CNS.

TGF-β2 mediates the inhibitory effect of NPCs on DC maturation. We next focused on identifying the secreted factor(s) responsible for the observed immunomodulatory effects of NPCs on inflammatory DCs.

First, we observed that NCM inhibits the production of IL-23 by CD40L-stimulated BMDCs in a dose-dependent manner (Supplemental Figure 7A). To investigate the nature of the secreted factor, NCM frozen at –20°C was thawed and then filtered through a 0.1-μm filter (Supplemental Figure 7B). The process did not alter NCM inhibitory activity, indicating that the factor is neither

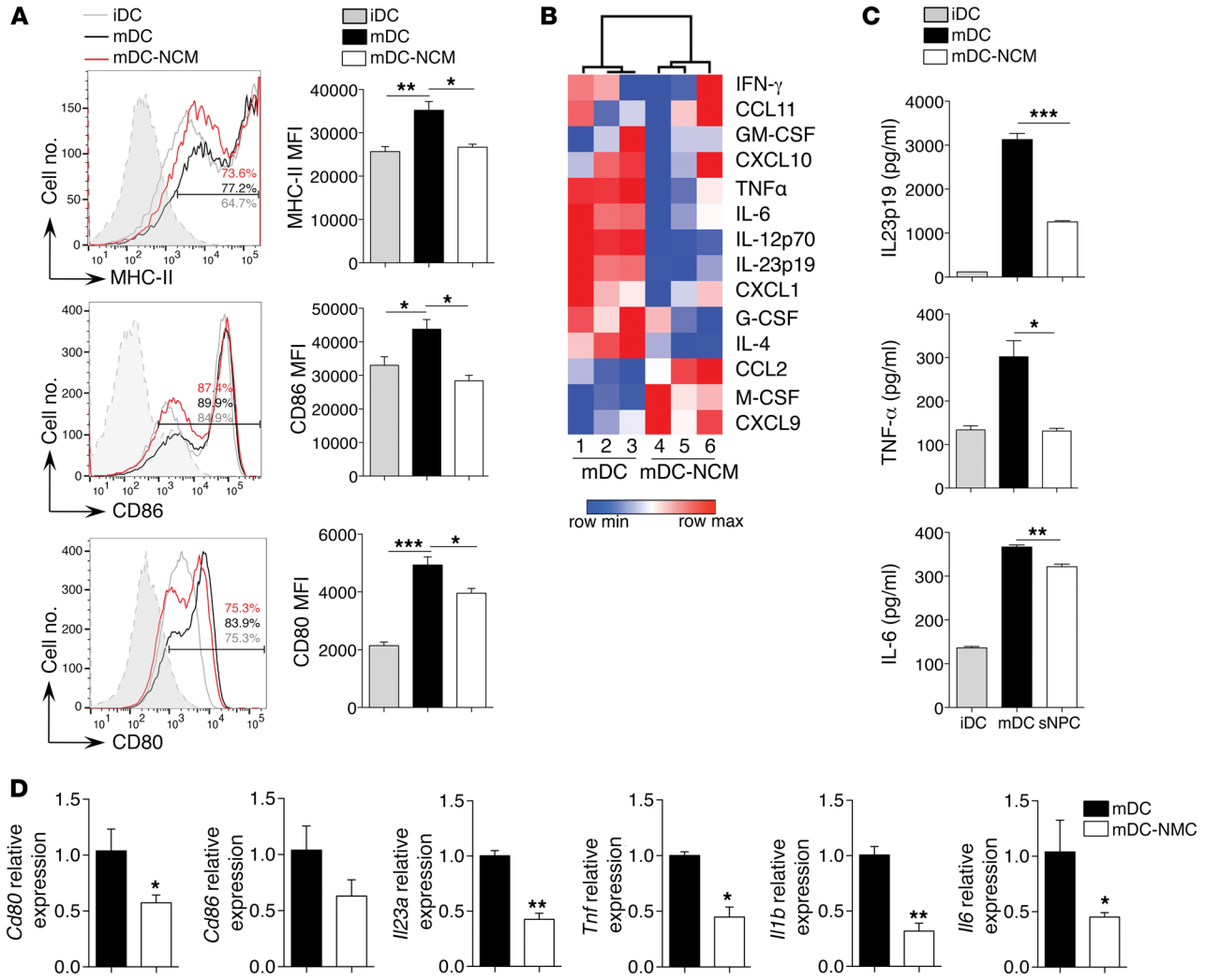

Figure 6. NPC-secreted factors impair the maturation of BMDCs. (**A**) Levels of MHC-II, CD86, and CD80 on CD40L-stimulated BMDCs in the absence or presence of NCM for 48 hours. Gray lines represent immature unstimulated BMDCs (iDCs), black lines BMDCs matured in control medium (mDC), red lines CD40L-matured BMDCs in the presence of NCM (mDC-NCM), and filled gray histograms fluorescence minus one controls (n = 3 samples per group). $^*P \le 0.05$, $^{**}P \le 0.01$, $^{***}P \le 0.001$, 1-way ANOVA with Bonferroni's post-test. (**B**) Unsupervised clustering of cytokine profile in supernatants of CD40L-matured BMDCs in the absence (mDC) or presence of NCM (mDC-NCM). Supernatants were collected after 48 hours in culture, 0.2-μm-filtered, and analyzed for expression of various cytokines by Luminex-based assay (individual samples are shown). (**C**) Protein levels of indicated cytokines in iDCs, mDC, and mDC-NCM, validated by ELISA (n = 3 samples per group). $^*P \le 0.05$, $^{**}P \le 0.01$, $^{***}P \le 0.001$, 1-way ANOVA with Bonferroni's post-test. (**D**) Expression of *Cd80*, *Cd86*, *Il23a*, *Il12b*, *Tnf*, *Il1b*, and *Il6* in BMDCs treated as in **B** for 18 hours, relative value to BMDCs matured in control medium (n = 3 samples per group). $^*P \le 0.05$, $^{**}P \le 0.01$, unpaired t test. $^*P \le 0.05$, $^{**}P \le 0.01$, $^{***}P \le 0.001$, 1-way ANOVA with Bonferroni's post-test. Gray bars, iDCs; black bars, mDC; white bars, mDC-NCM. Data are mean ± SEM and are representative of 2 independent experiments.

released as exosome nor as microvesicle. Further, size fractionation demonstrated that the inhibitory activity of NCM on DC maturation was absent when the secretome of ≤3 kDa was used, excluding small molecules as possible mediators of NCM effect (Supplemental Figure 7C). However, proteinase K treatment or heat inactivation (80°C) abolished NCM activity (Supplemental Figure 7D), indicating that the active secreted factor was a protein.

Since transcriptome analyses suggested the involvement of TGF-β signaling in the modulation of myeloid inflammatory cells by NPCs (Figures 8 and 9), we focused our investigation on elements of the TGF-β family, morphogenic factors with known immunomodulatory and tolerogenic effects on both T cells and DCs (54–58). NPCs release in vitro TGF-β2 and are equipped to promote activation of latent TGF-β2, via matrix metalloproteinases and thrombospondins (Figure 10, A and B). We further showed that BMDCs express receptors to transduce TGF-β signaling (Figure 10A). Supplementation of BMDC culture with TGF-β2 resulted in marked and dose-dependent inhibition of IL-23 secretion by CD40L-stimulated BMDCs (Figure 10C). Consistently, pharmacological inhibition of TGF-β signaling with SB431542, the tyrosine kinase inhibitor of TGF-β receptor 1 (TGFBRI), or with ITD1, which induces the proteosomal degradation of TGF-β receptor 2 (TGFBRII) (59), reverted almost completely the effect of NCM on DCs (Figure 10, D and E).

Furthermore, we confirmed that TGF-β2 signaling on BMDCs was required for NPC immunomodulation, since the

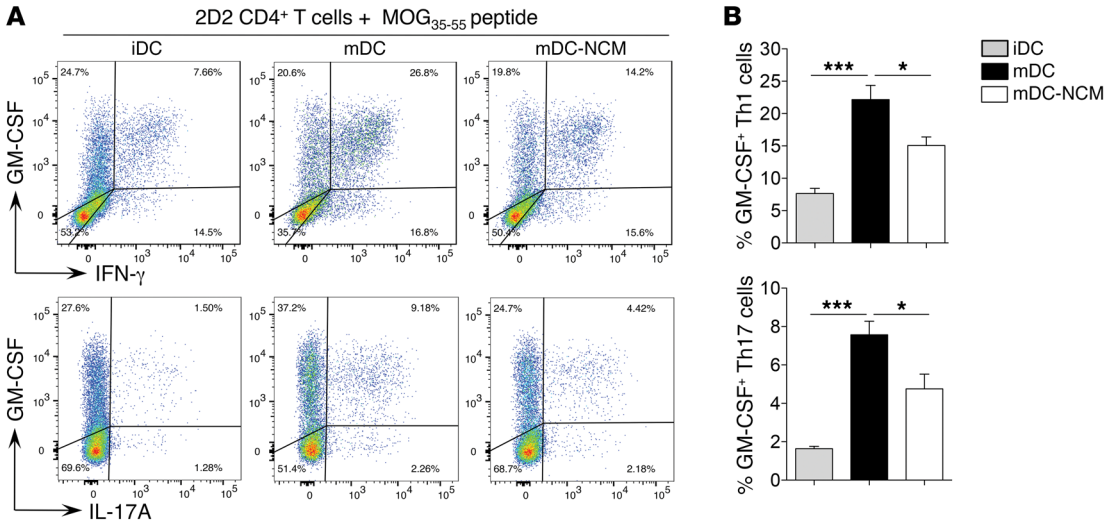

Figure 7. BMDCs matured in the presence of NPC-secreted factors fail to polarize MOG_{35-55}-specific $CD4^+$ T cells toward GM-CSF production. (**A** and **B**) Frequency of Th1 ($GM\text{-}CSF^+IFN\text{-}\gamma^+$) and Th17 ($GM\text{-}CSF^+IL\text{-}17^+$) among 2D2 $CD4^+$ T cells stimulated with MOG_{35-55} in the presence of BMDCs cultured as described in Figure 6 are shown in the plots (**A**) and graphs (**B**) (n = 3–4 samples per group). $^*P \le 0.05$, $^{***}P \le 0.001$, 1-way ANOVA with Bonferroni's post-test. Gray bars, iDCs; black bars, mDC; white bars, mDC-NCM. Data are mean ± SEM and are representative of 2 independent experiments.

genetic ablation of TGFBRII on $CD11c^+$ BMDCs, obtained from $CD11c\text{-}Cre^+Tgfbr2^{fl/fl}$ mice (60, 61), made DCs insensitive to the NCM effect (Figure 10F).

To investigate the role of TGF-β2, we generated NPCs from *Tgfb2tm1Doe* mice ($Tgfb2^{-/-}$), which constitutively lack functional TGF-β2 (62). Given the perinatal lethality of homozygous mutant mice (62), NPCs were derived from E15.5 $Tgfb2^{-/-}$ mouse embryos (embryonic NPCs [eNPCs]). $Tgfb2^{-/-}$ eNPCs were not affected in their viability and proliferative capacity in vitro (Supplemental Figure 8A); they efficiently differentiated in vitro into astrocytes and oligodendrocytes, producing slightly more neurons compared with WT ($Tgfb2^{+/+}$) eNPCs (Supplemental Figure 8, B–E). Importantly, $Tgfb2^{-/-}$ eNPCs maintained the expression of CD44, integrin α_4, and CXCR4 (Supplemental Figure 8F), adhesion molecules crucial for the homing and persistence of transplanted NPCs in the CNS during EAE (11).

The expression of TGF-β2 in eNPCs derived from heterozygous and homozygous *Tgfb2tm1Doe* mice was reduced in an allele-dosage manner at both the mRNA and the protein level (Figure 10, G and H). In line with this, NCM obtained from $Tgfb2^{-/-}$ eNPCs had significantly lower inhibitory activity on IL-23 production by BMDCs (Figure 10I).

Overall, these data pointed to TGF-β2 as the main driver of the immunomodulatory effect of NPC on BMDC differentiation and maturation.

TGF-β2 is nonredundant for the therapeutic effect of NPCs in chronic EAE. Upon intrathecal transplantation of NPCs in EAE mice, we observed that NPCs secrete TGF-β2 in vivo (Supplemental Figure 9, A and B) and that adjacent CNS-infiltrating $CD11b^+$ cells were positive for phosphorylated SMAD2 (p-SMAD2), suggestive of an activation of the TGF-β pathway in the MCs induced by NPC treatment (Supplemental Figure 9C).

To understand the therapeutic relevance of TGF-β2 produced by NPCs, we intrathecally transplanted $Tgfb2^{-/-}$ eNPCs in EAE mice. $Tgfb2^{-/-}$ eNPCs distributed within the perivascular space of the leptomeningeal vessels nearby inflammatory $CD11b^+$ cells, similarly to WT eNPCs ($Tgfb2^{+/+}$ eNPCs) (Figure 11, A and B). However, $Tgfb2^{-/-}$ eNPCs were not effective in inducing the clinical amelioration observed after WT eNPC transplantation (Figure 11C). Moreover, $Tgfb2^{-/-}$ eNPCs did not hamper demyelination, axonal damage, and inflammatory infiltration due to EAE (Figure 11, D–F). Consistently, $Tgfb2^{-/-}$ eNPCs failed to prevent accumulation of the inflammatory MCs in the CNS of EAE mice (Figure 11G) and upregulation of MHC-II on microglia (Figure 11H). Accordingly, WT NPC treatment, unlike $Tgfb2^{-/-}$ eNPC or PBS treatment, significantly increased the frequency of SMAD2 phosphorylation in CNS-infiltrating $CD11b^+$ myeloid cells, thus supporting that the therapeutic effect of NPCs acts through the activation of the TGF-β pathway in CNS-infiltrating MCs (Figure 11I).

We tried to recapitulate the therapeutic effect of NPCs via intrathecal injection in the cisterna magna of a lentiviral vector expressing TGF-β2. The resulting increased expression of TGF-β2 at the peak of EAE severity within the CNS was sufficient to induce clinical amelioration in EAE mice, when compared with control mice receiving GFP-expressing control lentiviral construct (Supplemental Figure 10).

Altogether our data indicate that TGF-β2 production by transplanted NPCs is necessary for NPC immunomodulatory effect on pathogenic properties of myeloid cells in vitro and in vivo and is nonredundant for NPC therapeutic effect in EAE.

Furthermore, increasing the intrathecal levels of TGF-β2 at the peak of EAE disease severity resulted in accelerated clinical recovery.

Discussion

In this study we provide evidence that intrathecally injected NPCs interfere with the pathogenic properties of CNS-infiltrating MCs via the secretion of the immunomodulatory cytokine TGF-β2.

Figure 8. NPC-secreted factors redirect the transcriptional program of BMDC maturation toward an alternative activation. (**A**) Workflow of microarray gene expression analysis at 6 and 18 hours showing the differential expression between control medium (mDC) and NCM-cultured BMDCs (mDC-NCM) during CD40L-induced maturation. (**B**) Unsupervised hierarchical clustering of expression profiles of 130 and 175 differentially modulated genes with ≥1.3-fold change and a $P \leq 0.01$ in mDC-NCM and mDC at 6 and 18 hours in culture, respectively, compared with the expression profiles of the same transcripts in unstimulated BMDCs (iDCs). Dashed lines indicate subclusters of genes that in mDC-NCM return to the expression levels observed in iDCs. (**C**) Gene ontology enrichment of differentially modulated genes between mDC-NCM and mDC at 6 and 18 hours. The gray scale indicates the statistical significance (FDR ≤0.05). (**D**) Color-coded ratio of mDC-NCM over mDC showing NCM-regulated genes at 18 hours, clustered to the indicated pathways (blue means downregulation, red upregulation). Significance is shown alongside. $^{*}P \leq 0.05$, $^{**}P \leq 0.01$, $^{***}P \leq 0.001$, unpaired *t* test. (**E** and **F**) Quantitative PCR validation of indicated differentially expressed genes in mDC-NCM compared with mDC at 6 (**E**) and 18 hours (**F**); the expression is relative to mDC ($n = 3$ samples per group). $^{*}P \leq 0.05$, $^{**}P \leq 0.01$, unpaired *t* test.

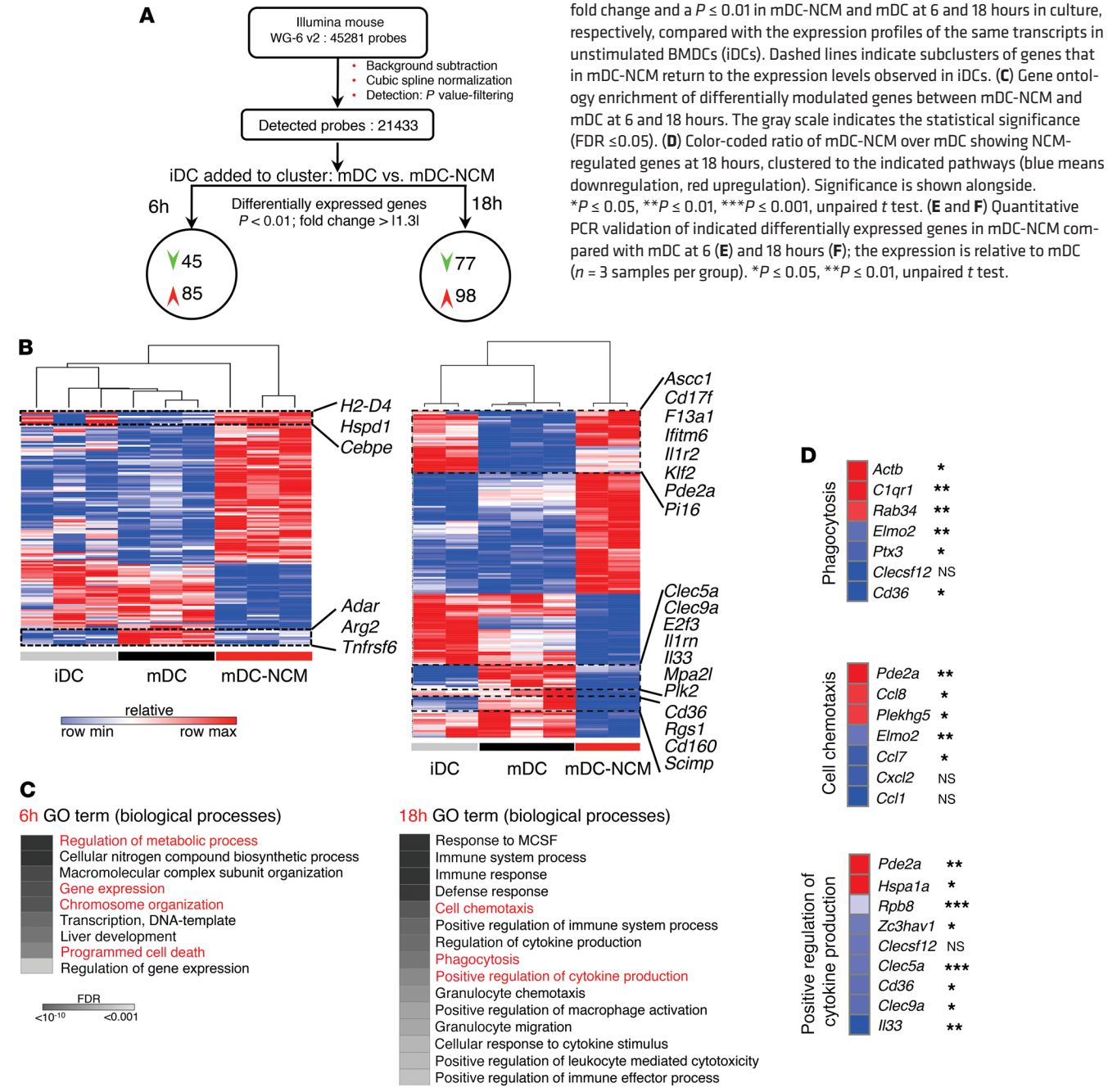

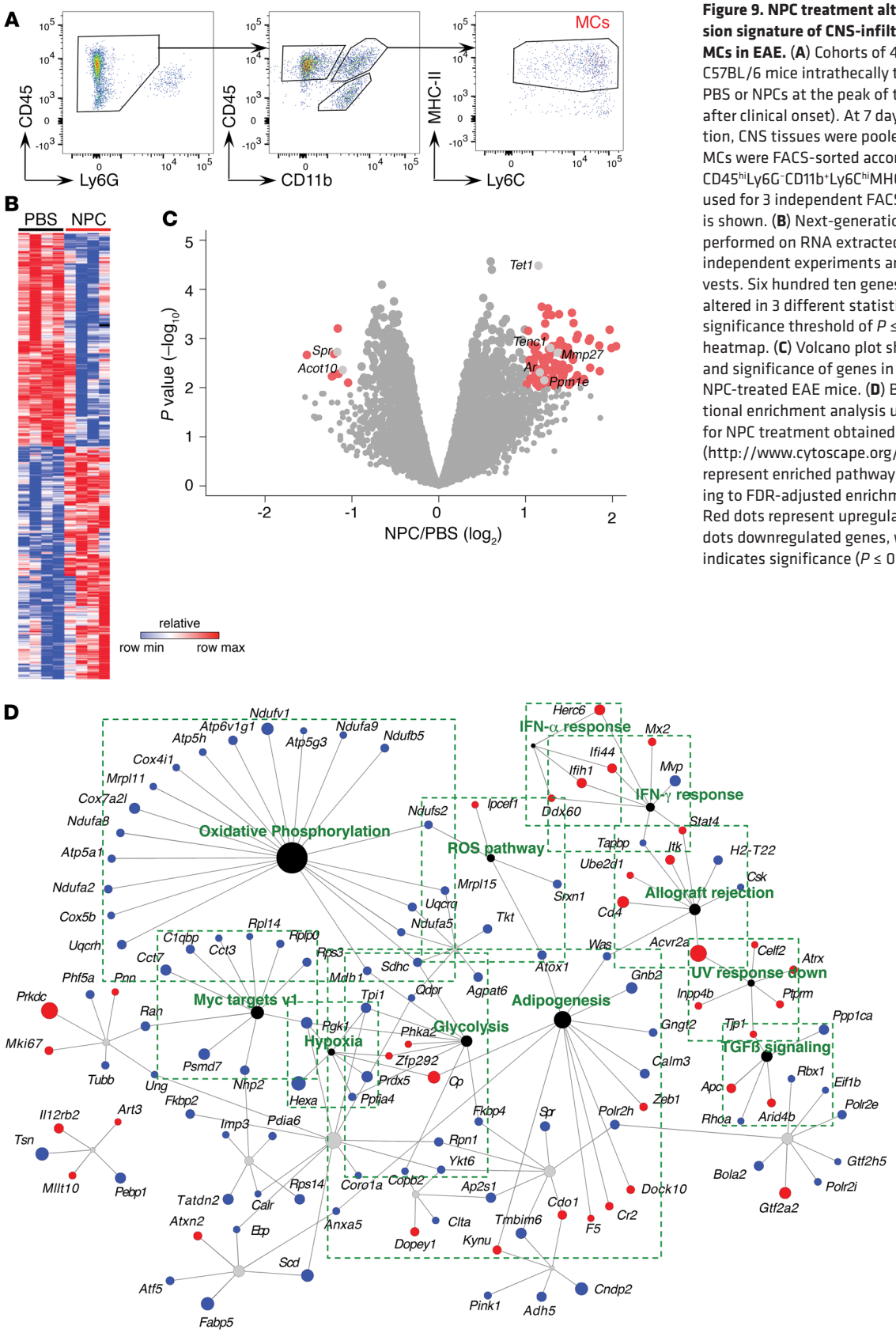

Figure 9. NPC treatment alters the gene expression signature of CNS-infiltrating inflammatory MCs in EAE. (**A**) Cohorts of 4–7 $MOG_{35–55}$-immunized C57BL/6 mice intrathecally treated with either PBS or NPCs at the peak of the disease (2–4 days after clinical onset). At 7 days after transplantation, CNS tissues were pooled and CNS-infiltrating MCs were FACS-sorted according to the phenotype $CD45^{hi}Ly6G^{-}CD11b^{+}Ly6C^{hi}MHC\text{-}II^{+}$. Sorting strategy used for 3 independent FACS sorting experiments is shown. (**B**) Next-generation sequencing was performed on RNA extracted from sorted cells of 3 independent experiments and respective CNS harvests. Six hundred ten genes that are significantly altered in 3 different statistical tests to a minimum significance threshold of $P \leq 0.01$ are shown in the heatmap. (**C**) Volcano plot showing the fold change and significance of genes in MCs from PBS- versus NPC-treated EAE mice. (**D**) Bipartite graph of functional enrichment analysis using hallmark data set for NPC treatment obtained by Cytoscape software (http://www.cytoscape.org/). Black and gray nodes represent enriched pathways with sizes corresponding to FDR-adjusted enrichment *P* value ($P \leq 0.05$). Red dots represent upregulated genes and blue dots downregulated genes, whereas the dot size indicates significance ($P \leq 0.01$).

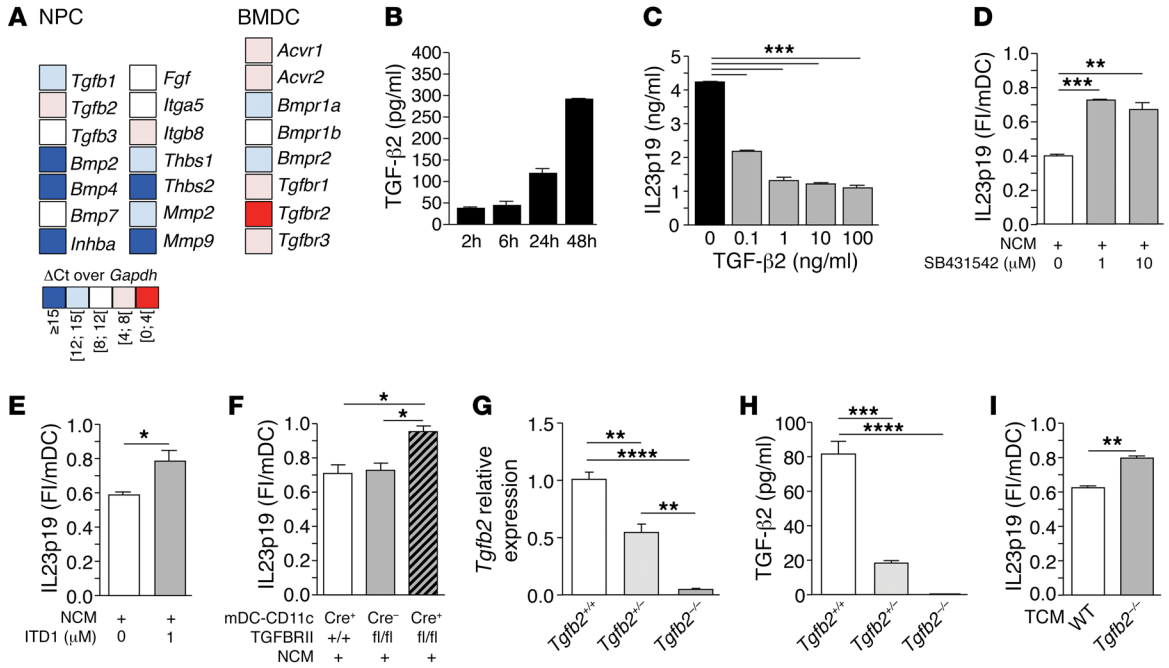

Figure 10. NPCs inhibit BMDC maturation in vitro via TGF-β2. (**A**) Color-coded expression heatmap of selected TGF-β family growth factors and TGF-β activating enzymes in NPCs (left) and of their relative receptors on mDC (CD40L-stimulated BMDCs; right). Data are represented as ΔCt over *Gapdh* (note that a higher ΔCt denotes a lower expression level). (**B**) ELISA for TGF-β2 performed on NCM from NPCs cultured in DC medium for 2, 6, 24, and 48 hours. (**C**) Quantification by ELISA of IL23p19 secreted in the supernatant of mDC cultured either in control medium (black bar) or in the presence of recombinant TGF-β2 at increasing concentrations (gray bars). (**D** and **E**) Quantification by ELISA of IL23p19 secreted by mDC cultured either in NCM alone (white bar) or in the presence of the TGFBRI tyrosine kinase inhibitor SB431542 (gray bars) (**D**) or with the TGFBRII inhibitor ITD1 (gray bar) (**E**). (**F**) Quantification by ELISA of the IL23p19 secreted by mDC from control littermates CD11c-Cre$^+$*Tgfbr2*$^{WT/WT}$ (white bar) and CD11c-Cre$^-$*Tgfbr2*$^{fl/fl}$ (gray bar) versus CD11c-Cre$^+$*Tgfbr2*$^{fl/fl}$ (gray striped bar) mDC lacking TGFBRII in CD11c$^+$ cells. Data in **D**-**F** are fold induction (FI) relative to mDC matured in control medium subjected to the same treatment. (**G**) Expression of *Tgfb2* mRNA in WT (*Tgfb2*$^{+/+}$), *Tgfb2*$^{+/-}$, and *Tgfb2*$^{-/-}$ eNPCs cultured for 48 hours in DCM relative to WT NPCs. (**H**) TGF-β2 protein quantification by ELISA secreted by *Tgfb2*$^{+/+}$, *Tgfb2*$^{+/-}$, and *Tgfb2*$^{-/-}$ eNPCs cultured for 48 hours in DC medium. (**I**) IL23p19 production (measured by ELISA) by mDC cultured in NCM from *Tgfb2*$^{+/+}$ (white bar) and *Tgfb2*$^{-/-}$ (gray bar) eNPCs. Data are FI relative to mDC matured in control medium. *$P \le 0.05$, **$P \le 0.01$, ***$P \le 0.001$, ****$P \le 0.0001$, 1-way ANOVA with Bonferroni's post-test (**C**, **D**, **F**, **H**, and **I**); *$P \le 0.05$, **$P \le 0.01$, ****$P \le 0.0001$, unpaired *t* test (**E**, **G**). Data are mean ± SEM and are representative of at least 2 independent experiments.

We initially observed that intrathecally transplanted NPCs distribute within the leptomeningeal perivascular space of EAE mice, close to myeloid infiltrating cells and pathogenic Th cells, and maintain mainly an undifferentiated phenotype. This localization within the leptomeninges, an important site for the reactivation of autoaggressive Th cells by meningeal perivascular macrophages (1), allows NPCs to impact on CNS-restricted immunopathogenic events.

Indeed, intrathecal transplantation of NPCs reduces during overt EAE the accumulation within the CNS of inflammatory infiltrating cells and in particular of monocytes and their progeny, MCs, and also restrains microglia activation, leading to a long-term amelioration of disease-related disability. Inflammatory Ly6C^{hi}-monocyte-derived DCs are indeed a key pathogenic myeloid cell population in the CNS of EAE mice (63, 64). EAE severity correlates with the number of monocytes in the spinal cord, and mice in which monocytes are inhibited from entering the CNS are protected against EAE development (35, 65, 66). The reduced infiltration of MCs in the CNS of NPC-treated mice and the evidence of lower microglia activation have been similarly observed in GM-CSF–depleted EAE mice (2, 67, 68). In fact, mice lacking GM-CSF do not develop EAE, since the accumulation of leukocytes is abolished, despite the initial CNS invasion by CD4$^+$ T cells (2, 69, 70).

Interestingly, we found that, early after treatment, NPC-injected EAE mice have reduced GM-CSF–producing pathogenic Th cells infiltrating the CNS and lower expression of genes related to Th17 pathogenic signature, including *Il23r*, essential for the maturation of effector Th17 cells (24, 71–74). The acquisition of Th17 pathogenic potential is a multistep process that starts in secondary lymphoid organs and can be completed only in the target tissue (75). MCs act as blood-borne APCs, sustaining encephalitogenic Th cell reactivation and full differentiation within the inflamed CNS through the secretion of proinflammatory cytokines (4, 5, 7, 63). Our data reveal that NPC treatment reduces in the CNS the burden of polarizing cytokines, including IL-1 and IL-23, required for the generation of pathogenic GM-CSF–producing Th cells.

Considering that intrathecally transplanted NPCs maintain an undifferentiated phenotype, we hypothesized a paracrine effect of NPCs, acting via the secretion of cytokines, growth factors, or morphogens to modulate infiltrating myeloid inflammatory cells. Accordingly, NPC-secreted factors recapitulated in vitro the NPC inhibitory effect on the ability of DCs to secrete polarizing cyto-

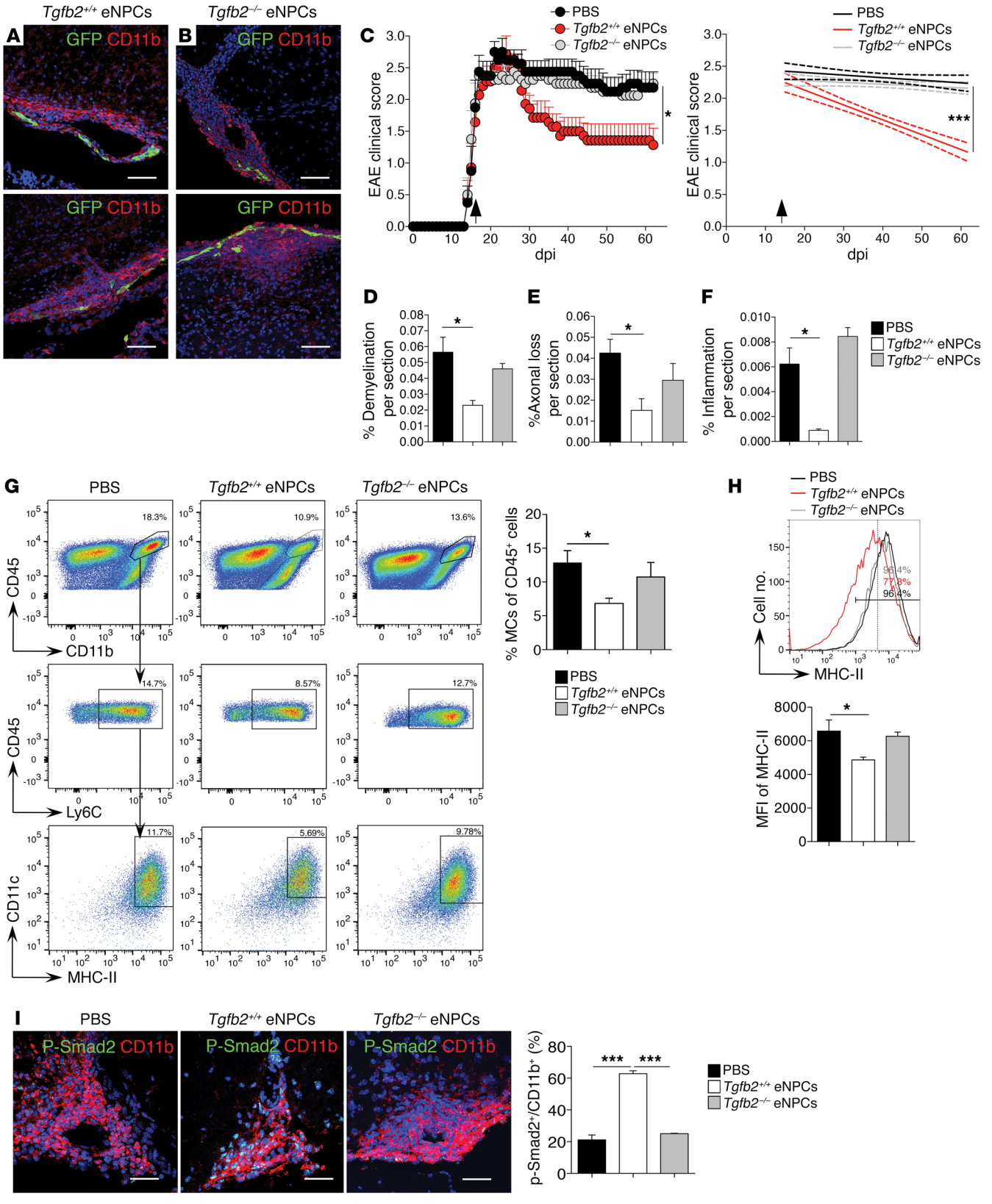
Tgfb2+/+ eNPCs
Tgfb2−/− eNPCs
A
B
GFP CD11b
C
PBS
Tgfb2+/+ eNPCs
Tgfb2−/− eNPCs
EAE clinical score
dpi
*
***
D
% Demyelination per section
E
%Axonal loss per section
F
% Inflammation per section
G
CD45
CD11b
Ly6C
CD11c
MHC-II
18.3%
10.9%
13.6%
14.7%
8.57%
12.7%
11.7%
5.69%
9.78%
% MCs of CD45+ cells
H
Cell no.
96.4%
77.8%
96.4%
MFI of MHC-II
I
P-Smad2 CD11b
p-Smad2+/CD11b+ (%)

Figure 11. NPC-secreted TGF-β2 is nonredundant for the therapeutic effect. (**A** and **B**) Representative immunostainings showing similar localization of GFP$^+$ *Tgfb2*$^{+/+}$ (**A**) and *Tgfb2*$^{-/-}$ (**B**) eNPCs (green) in meningeal perivascular areas in proximity to CD11b$^+$ cells (red). Nuclei stained with DAPI (blue). Scale bars: 25 μm. (**C**) Left: Clinical scores of EAE mice treated with intrathecal injection of PBS (black dots), *Tgfb2*$^{+/+}$ eNPCs (red dots), or *Tgfb2*$^{-/-}$ eNPCs (gray dots) at the peak of the disease (arrow) (n = 10 mice per group). Each point represents the mean ± SEM. *$P \le 0.05$, 2-way ANOVA with Bonferroni's post-test. Right: Linear regression curves from day of treatment (18 dpi); dashed lines indicate 95% CI. ***$P \le 0.001$. (**D**–**F**) Quantification of spinal cord demyelination (Luxol fast blue staining) (**D**), axonal loss (Bielschowsky silver staining) (**E**), and inflammatory infiltration (H&E staining) (**F**) at 60 dpi in EAE mice treated with *Tgfb2*$^{-/-}$ eNPCs (gray bars), *Tgfb2*$^{+/+}$ eNPCs (white bars), and PBS (black bars) (n = 20 sections per mouse, 4 mice per group). Data are mean ± SEM and represent the percentage area of damage per total section area. *$P \le 0.05$, unpaired t test. (**G**) Flow cytometry of CNS leukocytes from EAE mice treated as in **C**, assessed at day 7 after transplantation (n = 4 mice per group). Frequencies of inflammatory MCs (CD45^{hi}CD11b$^+$Ly6G$^-$Ly6C^{hi}CD11c$^+$MHC-II$^+$) are shown in the plots and quantified in the graph. Black bars, PBS; white bars, *Tgfb2*$^{+/+}$ eNPCs; gray bars, *Tgfb2*$^{-/-}$ eNPCs. (**H**) Levels of MHC-II on microglia in EAE mice treated with PBS (black line), *Tgfb2*$^{+/+}$ eNPCs (red line), and *Tgfb2*$^{-/-}$ eNPCs (gray line) at the same time point as **I** are shown in the histogram and quantified in the graph (n = 4 per group). *$P \le 0.05$, 1-way ANOVA followed by Bonferroni's post-test. (**I**) Confocal images and frequency of phospho-SMAD2$^+$ cells over CD11b$^+$ cells in the spinal cord of EAE mice treated with PBS, *Tgfb2*$^{+/+}$ eNPCs, and *Tgfb2*$^{-/-}$ eNPCs, 7 days after treatment (n = 8–12 inflammatory infiltrates per mouse; n = 3 mice per group). ***$P \le 0.001$, 1-way ANOVA followed by Bonferroni's post-test. Data are mean ± SEM and are representative of 2 independent experiments.

kines, including IL-23, IL12p70, TNF-α, and IL-1β, and to drive the differentiation of GM-CSF–producing pathogenic Th cells.

Transcriptome analyses revealed that NPC-secreted factors induce a profound rearrangement of chromatin organization, metabolism, and biosynthetic processes in myeloid cells. These modifications lead to the reprogramming of inflammatory DCs toward an alternative activation state, defined by the downregulation of proinflammatory chemokines (*Ccl1*, *Ccl2*, *Ccl3*, *Ccl7*, *Ccl8*, *Cxcl2*) (35) and of positive regulators of cytokine production (*Cd36*, refs. 36, 37; *Il33*, ref. 38; *Clec9a*, ref. 39; and *Clec5a*) and by the upregulation of tolerogenic genes, such as hepcidin (76), *Il1r2* (41), and *Ascc1* (42).

Interestingly, transcription factor analyses suggested that the effect of NPCs on MCs might involve the activation of c-Myc, c/EBPβ, and CREB1, known to control M2 polarization and MDSC differentiation (45, 77), as well as the inhibition of PU.1, known to maintain the identity and inflammatory phenotype of DCs (46, 78). Gene set enrichment analysis confirmed that NPC treatment of EAE promoted in CNS-invading MCs a program of alternative activation via c-Myc activation and indicated TGF-β signaling as a possible upstream coordinator of the NPC-dependent antiinflammatory polarization of CNS-infiltrating MCs.

In line with our findings, a recent report has demonstrated that the upregulation of inhibitor of differentiation 1 (ID1), in response to tumor-derived factors, including TGF-β, is responsible for the switch from DC differentiation to MDSC expansion during tumor progression (78). In fact, the generation of the 2 tolerogenic myeloid cell populations, MDSCs and tumor-associated macrophages, in tumor-bearing hosts requires the integration of at least 2 types of signals: factors that expand myeloid precursors such as M-CSF, G-CSF, and GM-CSF (79), followed by factors that activate immune-regulatory programs. Besides classic Th2 cytokines (e.g., IL-4 and IL-13), chemokines (e.g., CCL5, CXCL12, and CX3CL1) as well as growth factors and noncanonical chemotactic peptides (e.g., VEGF-α, TGF-β, basic FGF, and antimicrobial peptides) (80) can contribute as "second signal" to monocyte recruitment and tolerogenic macrophage differentiation (45). In our study of intrathecal NPC treatment during the effector phase of EAE, we hypothesized that the inflammatory milieu provides abundant proliferative stimuli to the CNS-infiltrating myeloid compartment, while NPC-secreted TGF-β2 could impart the antiinflammatory signal. TGF-β signaling is necessary to prevent autoimmunity (81), and the signaling through the TGFBRs in DCs is a prerequisite to control EAE autoimmune response (82). Moreover, TGF-β limits at the site of inflammation the differentiation of highly mature DCs as a means of restricting Th17 cell differentiation and controlling autoimmunity (83).

In our experimental setting, TGF-β2 was found to be the most expressed among TGF-β family members in NPCs, and gain- and loss-of-function experiments demonstrated that TGF-β2 recapitulates the immunomodulatory effect of NPCs in vitro. In support of the role of TGF-β2, the transplantation of TGF-β2–deficient NPCs, during the EAE effector phase, failed to induce the expected clinical and neuropathological improvement, since it did not prevent the accumulation of MCs in the CNS. This finding indicates that TGF-β2 is required for efficient immunomodulation by transplanted NPCs, since a different source of NPCs (eNPCs), lacking only TGF-β2, did not display a therapeutic effect in our experimental setting. Moreover, increasing TGF-β2 levels in the CNS with intrathecally targeted gene therapy significantly ameliorated the chronic phase of EAE. TGF-β2 is constitutively expressed by astrocytes in the adult CNS, and little is known about its function during neuroinflammation. It has been suggested that TGF-β2 plays a central role in the maintenance of CNS immune privilege, and downregulation of astrocyte-derived TGF-β2 by T cell– and myeloid-secreted inflammatory cytokines appears to be a critical step for the induction and maintenance of neuroinflammation (84–86).

Altogether our data prove that increasing TGF-β signaling in the CNS is sufficient to interfere with differentiation and activation of MCs, which are recognized as the primary cell population sustaining neuroinflammation and the final effectors of tissue damage in CNS autoimmunity. In line with our findings, a recent work demonstrated that the selective deletion of TGFBRII in moDCs leads to the retention of moDCs in the CNS and to the development of more severe chronic EAE with increased irreversible tissue damage and no remission (87).

Compelling evidence demonstrates how ablating monocytes in the effector phases of EAE ameliorates disease progression and disability (35, 88). However, a phase II clinical trial with MLN1202, a human antibody blocking CCR2, failed to induce clinical amelioration in MS patients (3). A possible explanation is that this antibody could mainly act via peripheral ablation of monocytes, many of which, at this time point, might have already migrated into the CNS and undergone local differentiation and activation (3). Instead, a successful myeloid-directed therapeutic strategy in established CNS autoimmunity might focus on modulating in the

CNS the differentiation and activation of MCs, rather than ablating their entry from the periphery (3).

In conclusion, we here propose, for the first time to our knowledge, a treatment able to target CNS-restricted pathogenic mechanisms of EAE effector phase. We identify TGF-β2 as the nonredundant secreted mediator of NPC immunomodulation in the inflamed CNS and as a potent immunomodulatory cytokine able to reprogram proinflammatory MCs to antiinflammatory/suppressive-like myeloid cells. The reduced amount of MC-derived polarizing cytokines and proinflammatory mediators in the CNS limits tissue damage and inhibits the terminal differentiation of pathogenic GM-CSF–producing Th cells. The reduction of GM-CSF levels acts synergistically with TGF-β2 in the CNS to impair the effector properties of MCs, disrupting the positive-feedback loop sustaining leukocyte recruitment and tissue damage in EAE. This allows accelerated recovery and significantly less accumulation of irreversible axonal loss in the chronic phase of the disease.

Methods

Mice. C57BL/6 female mice 6–8 weeks old were purchased from Charles River Italy. Mice with a transgene expressing T cell receptor specific for $MOG_{35–55}$ (2D2 mice; The Jackson Laboratory) (89) were provided by R. Furlan from the San Raffaele Scientific Institute. B6.Cg-Tg(Itgax-cre)1-1Reiz/J mice (The Jackson Laboratory) (61) expressing Cre recombinase under the CD11c promoter were obtained from M. Falcone from the San Raffaele Scientific Institute. B6;129-*Tgfbr2*tm1Karl/J mice (The Jackson Laboratory) (60) were provided by M. Greter (University of Zürich, Zürich, Switzerland). Heterozygous *Tgfb2*tm1Doe/J mice were kindly provided by T. Doetschman (University of Arizona, Tucson, Arizona, USA) (62).

Adult and embryonic mouse NPC culture. Mouse NPCs were obtained as previously described from dissected subventricular zone of adult (6- to 8-week-old) C57BL/6 female mice (NPCs) (14) and from dissected cortex of E15.5 C57BL/6 embryos (embryonic NPCs [eNPCs]) (90) from $Tgfb2^{-/-}$ and $Tgfb2^{+/+}$ mice. Details are provided in Supplemental Methods.

In vitro differentiation and activation of BMDCs. BMDCs were prepared from bone marrow cell suspension from flushed tibias and femurs of naive C57BL/6 mice as previously described (91, 92). At day 6 of in vitro culture, BMDCs were used to investigate CD40L-induced DC maturation: BMDCs were plated at the concentration of 2×10^6 per milliliter in the presence of recombinant CD40L (10 μg/ml; R&D Systems) in DCM or NCM. In most of the experiments, BMDCs and culture supernatants were collected at 48 hours for FACS analysis and cytokine measurements, respectively. For gene expression analysis, BMDCs were harvested at 6 and 18 hours.

In indicated experiments the following cytokines or pharmacological inhibitors were added at the indicated concentrations: TGF-β2 (R&D Systems), SB431542 (Tocris), and ITD1 (Tocris). In a set of experiments, BMDCs were derived from transgenic CD11c-$Cre^+Tgfbr2^{fl/fl}$, CD11c-$Cre^+Tgfbr2^{WT/WT}$, and CD11c-$Cre^-Tgfbr2^{fl/fl}$ mice obtained by in-house breeding. Since CD11c$^-$Cre$^+$*Tgfbr2*$^{fl/fl}$ animals develop a severe, often fatal, autoimmune disease after 8 weeks of age, these mice were used before 8 weeks of age for ethical issues (60). To obtain a pure population of CD11c$^+$ cells in which TGFBRII had been deleted, BMDCs derived from these latter 3 genotypes were FACS-sorted (Moflo XDP, Beckman Coulter) (achieving a 97% of purity) before being seeded for CD40L stimulation.

Myelin antigen presentation assay. Fifty thousand BMDCs, matured with CD40L in vitro (10 μg/ml; R&D Systems) for 48 hours in NCM or DCM, were cultured in IMDM medium with 10% FCS (Genenco), 2 mM L-glutamine (BioWhittaker), 100 U/ml penicillin, 100 mg/ml streptomycin (BioWhittaker), 50 mM 2-mercaptoethanol (Lonza) with 2×10^5 CD4$^+$ T cells isolated by CD4$^+$ T cell MACS beads (Miltenyi Biotec), according to the manufacturer's procedures, from splenocytes of $MOG_{35–55}$-immunized 2D2 mice at 7 dpi in the presence of $MOG_{35–55}$ peptide (20 μg/ml; Espikem) for 72 hours. DCs/CD4$^+$ T cells were harvested and analyzed for cytokine production by flow cytometry.

Cytokine analysis. Multiplex quantification of cytokines and chemokines in BMDC supernatant and in CNS lysates from EAE mice was performed using a custom 16-plex Luminex plate (R&D Systems) according to the manufacturer's recommendations. Unsupervised clustering was performed on normalized, median-centered data and reported as heatmap using GENE-E software (Broad Institute). For IL23p19, GM-CSF, TGF-β2, TNF-α, and IL-6, ELISA was performed (DuoSet ELISA kit, R&D Systems) according to the manufacturer's instructions.

Gene expression microarray. Total RNA was isolated from at least 2×10^6 BMDCs unstimulated (iDCs) or stimulated with CD40L in DCM (mDC) or NCM (mDC-NCM) at 6 and 18 hours of culture using the RNeasy Mini Kit (Qiagen). RNA quality was confirmed with a 2100 Bioanalyzer (Agilent). cRNA amplification was performed using the Illumina TotalPrep RNA Amplification Kit (Ambion), and 1.5 μg of biotin-labeled cRNA of each sample was hybridized on Illumina MouseWG-6 v2 Expression BeadChip (Illumina). Data were deposited at ArrayExpress with the accession number E-MTAB-5307. Details on bioinformatics analysis are provided in Supplemental Methods.

Next-generation sequencing. C57BL/6 mice were immunized and treated with NPC or PBS at the peak of disease as described above. Seven days after transplantation, CD45^{hi}CD11b$^+$Ly6C^{hi}Ly6G$^-$MHC-II$^+$ MCs were FACS-sorted (BD FACSAria III) from hindbrain and spinal cord as described above. Total RNA from a minimum of 3×10^5 up to 5×10^5 cells was isolated with Qiagen RNeasy Plus Micro Kit according to the manufacturer's instructions. RNA quality was confirmed with a 2100 Bioanalyzer (Agilent) resulting in RNA integrity number ≥8. Amplification of cDNA from total RNA was performed using the Ovation RNA-Seq system V2 (NuGEN). Then, cDNA was fragmented and ligated into a sequencing library using Ovation Ultralow Library System V2 (NuGEN). Libraries were PCR-amplified for 12 cycles and sequenced on an Illumina NextSeq 500 System with TruSeq reagent kits and software. Data were deposited at the NCBI's Gene Expression Omnibus (GEO) database with the accession number GSE92395. Details on bioinformatics analysis are provided in Supplemental Methods.

EAE induction. Chronic EAE was induced in 6- to 8-week-old C57BL/6 female mice by s.c. immunization of $MOG_{35–55}$ peptide (200 μg per mouse) in incomplete Freund's adjuvant containing 4 mg/ml of *Mycobacterium tuberculosis*. Pertussis toxin (500 ng) was injected i.v. at 0 and 2 dpi. The animals were assessed daily for body weight and clinical symptoms of EAE. Their disease stage was recorded by 3 researchers blinded to the treatment with the following scoring system (14): 0, healthy; 1, limp tail; 1.5, wobbling gait; 2, slight paresis of hind limbs/difficulty in righting; 2.5, severe paralysis of hind limbs; 3, complete paralysis of hind limbs; 3.5, initial paresis of forelimbs; 4, tetraparalysis; 5, death.

NPC intrathecal transplantation. At the treatment day, 4 days after clinical onset of EAE, animals were randomized into treatment groups and anesthetized with i.p. injection of 120–200 μl of 12.5% ketamine

and 6.25% xylazine in 0.9% saline solution. Animals were fixed on a stereotactic device (David Kopf Instruments). A 10-μl Hamilton syringe was loaded either with 10^6 NPCs, WT eNPCs, or *Tgfb2*$^{-/-}$ eNPCs diluted in 10 μl of PBS or with control vehicle solution (PBS), according to experimental requirements. The Hamilton syringe was then stereotactically placed between the atlas and occipital bone at 35°, and advanced to puncture the cisterna magna. The following stereotactic coordinates were used: $x = 0$; $y = -7.5$ mm from λ; $z = -4.5$ mm from muscle plane. A total volume of 10 μl was injected in a 5-minute time period.

Isolation of CNS leukocytes. Extracted CNS tissue was cut into small pieces, incubated for 30 minutes with 0.2 mg/ml collagenase type IV (Sigma-Aldrich), and afterward passed through a 19G syringe to obtain a homogeneous cell suspension. CNS cell suspensions were further enriched by a Percoll gradient as previously described (93).

Flow cytometry, intracellular staining, and sorting. Flow cytometry was performed using a CantoII (Becton Dickinson) flow cytometer and analyzed with FlowJo software (Tree Star). FACS sorting was performed on BD FACSAria III (Becton Dickinson) or Moflo XDP (Beckman Coulter). Fluorochrome-conjugated mAbs specific for mouse MHC class II I-A/I-E (clone M5/114.15.2), CD11b (clone M1/70), CD11c (clone N418), CD45 (clone 30-F11), Ly6C (clone AL-21), Ly6G (clone 1A8), CD4 (clone GK1.5), CD3 (clone 17A2), CD80 (clone 16-10A1), and CD86 (clone GL1) were purchased from either BD Biosciences, eBioscience, or Biolegend.

For intracellular staining of T cell cytokines, cells were stimulated for 6 hours with phorbol 12-myristate 13-acetate (50 ng/ml) and ionomycin (500 ng/ml) in the presence of GolgiPlug (1:1,000; BD Pharmingen). Cells were first stained for surface molecules, fixed and permeabilized with a Cytofix/Cytoperm Plus kit (BD Biosciences), and stained with the following fluorochrome-conjugated mAbs: GM-CSF (clone MP1-22E9), IL-17A (clone TC11-18H10), and IFN-γ (clone XMG1.2) from BD Pharmingen. For analysis of intracellular FoxP3, cell preparations were stained for cell surface markers, then were fixed and made permeable with fixation-permeabilization buffers (eBioscience) and stained with fluorochrome-conjugated anti-FoxP3 mAb (clone FJK-16s) from eBioscience.

Dead cells were always excluded using a LIVE/DEAD stain kit (Invitrogen).

Histopathological analyses and immunofluorescence stainings. Details are provided in Supplemental Methods.

Statistics. Real-time PCR data, FACS data, EAE score, and histology results are expressed as mean ± SEM. Results were analyzed using the unpaired 2-tailed Student's *t* test or 1-way ANOVA with Bonferroni's post-test except for clinical score, which was assessed by 2-way ANOVA with Bonferroni's post-test and linear regression. Analyses were performed using Prism v5.0a software (GraphPad). Statistical significance was accepted for P less than or equal to 0.05.

Study approval. All mouse experiments were conducted with approval from the Institutional Animal Committee of the San Raffaele Scientific Institute (IACUC number 568).

Further method descriptions are provided in the Supplemental Methods section.

Author contributions

DD designed and performed experiments, evaluated and interpreted data, and wrote the manuscript. AM performed histology and biochemical experiments, evaluated and interpreted data, and contributed to manuscript preparation. E Brambilla performed experiments. LO, RM, SS, and CF performed microarray bioinformatics analyses. CL helped in transplantation experiments and the microarray experiment. JMGM and LO performed RNA-Seq analyses. E Butti prepared the lentiviral constructs. MB performed experiments and edited the manuscript. GC reviewed the manuscript. MG provided transgenic mouse lines, performed the cell sorting experiment, and edited the manuscript. GM supervised and financed the study and edited the manuscript.

Acknowledgments

We thank the Center for Translational Genomics and BioInformatics, San Raffaele Scientific Institute, for RNA sequencing and bioinformatics analysis; Advanced Light and Electron Microscopy BioImaging Center, San Raffaele Scientific Institute, for the use of equipment; the Center for Microscopy and Image Analysis, University of Zürich, for the use of equipment; the Mouse HistoPathology Unit, San Raffaele Scientific Institute, for support and equipment usage for immunohistochemistry; F. Ruffini and A. Finardi, San Raffaele Scientific Institute, for technical assistance; Thomas Doetschman, University of Arizona, for providing the *Tgfb2*-knockout strain; V. Tosevski, University of Zürich, for technical help and FACS sorting; and A. Cantore, TIGET San Raffaele Scientific Institute, for *Tgfb2*-expressing lentiviral vector production. This work has been in part supported by TargetBrain (EU Framework 7 project HEALTH-F2-2012–279017), by NEUROKINE network (EU Framework 7 ITN project), by BMW Italy Group, by Fondazione Italiana Sclerosi Multipla (FISM) n the project entitled Progetto Speciale Cellule Staminali, and by CARIPLO Foundation grant no. 2010 1835 to GM and by Ministero della Salute Italiana (Progetto Giovani Ricercatori 58/GR-2011-02348160) to MB.

Address correspondence to: Gianvito Martino, Institute of Experimental Neurology, Division of Neuroscience, San Raffaele Scientific Institute, Via Olgettina 58, 20132 Milan, Italy. Phone: 390226434958; Email: martino.gianvito@hsr.it.

DD's present address is: Institute of Experimental Immunology, University of Zürich, Zürich, Switzerland.

CL's present address is: Laboratory of Stem Cells and Restorative Neurology, Lund Stem Cell Center, University Hospital, Lund, Sweden.

RM's present address is: Scientist–Bioinformatics Division, MedGenome Labs Pvt. Ltd., Narayana Health City, Bommasandra, India.

1. Bartholomäus I, et al. Effector T cell interactions with meningeal vascular structures in nascent autoimmune CNS lesions. *Nature*. 2009;462(7269):94–98.
2. Codarri L, et al. RORγt drives production of the cytokine GM-CSF in helper T cells, which is essential for the effector phase of autoimmune neuroinflammation. *Nat Immunol*. 2011;12(6):560–567.
3. Croxford AL, et al. The cytokine GM-CSF drives the inflammatory signature of CCR2+ monocytes and licenses autoimmunity. *Immunity*. 2015;43(3):502–514.
4. Greter M, et al. Dendritic cells permit immune invasion of the CNS in an animal model of multiple sclerosis. *Nat Med*. 2005;11(3):328–334.
5. Bailey SL, Schreiner B, McMahon EJ, Miller SD. CNS myeloid DCs presenting endogenous

myelin peptides 'preferentially' polarize CD4+ T(H)-17 cells in relapsing EAE. *Nat Immunol*. 2007;8(2):172–180.
6. Becher B, Segal BM. T(H)17 cytokines in autoimmune neuro-inflammation. *Curr Opin Immunol*. 2011;23(6):707–712.
7. Ko HJ, et al. GM-CSF-responsive monocyte-derived dendritic cells are pivotal in Th17 pathogenesis. *J Immunol*. 2014;192(5):2202–2209.
8. Yamasaki R, et al. Differential roles of microglia and monocytes in the inflamed central nervous system. *J Exp Med*. 2014;211(8):1533–1549.
9. Haghikia A, Hohlfeld R, Gold R, Fugger L. Therapies for multiple sclerosis: translational achievements and outstanding needs. *Trends Mol Med*. 2013;19(5):309–319.
10. Hemmer B, Kerschensteiner M, Korn T. Role of the innate and adaptive immune responses in the course of multiple sclerosis. *Lancet Neurol*. 2015;14(4):406–419.
11. Pluchino S, et al. Neurosphere-derived multipotent precursors promote neuroprotection by an immunomodulatory mechanism. *Nature*. 2005;436(7048):266–271.
12. Martino G, Pluchino S. The therapeutic potential of neural stem cells. *Nat Rev Neurosci*. 2006;7(5):395–406.
13. De Feo D, Merlini A, Laterza C, Martino G. Neural stem cell transplantation in central nervous system disorders: from cell replacement to neuroprotection. *Curr Opin Neurol*. 2012;25(3):322–333.
14. Pluchino S, et al. Injection of adult neurospheres induces recovery in a chronic model of multiple sclerosis. *Nature*. 2003;422(6933):688–694.
15. Imitola J, et al. Directed migration of neural stem cells to sites of CNS injury by the stromal cell-derived factor 1α/CXC chemokine receptor 4 pathway. *Proc Natl Acad Sci U S A*. 2004;101(52):18117–18122.
16. Bacigaluppi M, et al. Delayed post-ischaemic neuroprotection following systemic neural stem cell transplantation involves multiple mechanisms. *Brain*. 2009;132(pt 8):2239–2251.
17. Cusimano M, et al. Transplanted neural stem/precursor cells instruct phagocytes and reduce secondary tissue damage in the injured spinal cord. *Brain*. 2012;135(pt 2):447–460.
18. Mosher KI, et al. Neural progenitor cells regulate microglia functions and activity. *Nat Neurosci*. 2012;15(11):1485–1487.
19. Cao W, et al. Leukemia inhibitory factor inhibits T helper 17 cell differentiation and confers treatment effects of neural progenitor cell therapy in autoimmune disease. *Immunity*. 2011;35(2):273–284.
20. Ottoboni L, De Feo D, Merlini A, Martino G. Commonalities in immune modulation between mesenchymal stem cells (MSCs) and neural stem/precursor cells (NPCs). *Immunol Lett*. 2015;168(2):228–239.
21. Einstein O, et al. Intraventricular transplantation of neural precursor cell spheres attenuates acute experimental allergic encephalomyelitis. *Mol Cell Neurosci*. 2003;24(4):1074–1082.
22. Laterza C, et al. iPSC-derived neural precursors exert a neuroprotective role in immune-mediated demyelination via the secretion of LIF. *Nat Commun*. 2013;4:2597.
23. Guilliams M, et al. Dendritic cells, monocytes and macrophages: a unified nomenclature based on ontogeny. *Nat Rev Immunol*. 2014;14(8):571–578.
24. Lee Y, et al. Induction and molecular signature of pathogenic TH17 cells. *Nat Immunol*. 2012;13(10):991–999.
25. El-Behi M, et al. The encephalitogenicity of T(H)17 cells is dependent on IL-1- and IL-23-induced production of the cytokine GM-CSF. *Nat Immunol*. 2011;12(6):568–575.
26. Rissone A, et al. Reticular dysgenesis-associated AK2 protects hematopoietic stem and progenitor cell development from oxidative stress. *J Exp Med*. 2015;212(8):1185–1202.
27. Király R, Demény M, Fésüs L. Protein transamidation by transglutaminase 2 in cells: a disputed Ca^{2+}-dependent action of a multifunctional protein. *FEBS J*. 2011;278(24):4717–4739.
28. Jablonski KA, et al. Novel markers to delineate murine M1 and M2 macrophages. *PLoS One*. 2015;10(12):e0145342.
29. Cao S, Liu J, Song L, Ma X. The protooncogene c-Maf is an essential transcription factor for IL-10 gene expression in macrophages. *J Immunol*. 2005;174(6):3484–3492.
30. Ahmed N, et al. The E3 ligase Itch and deubiquitinase Cyld act together to regulate Tak1 and inflammation. *Nat Immunol*. 2011;12(12):1176–1183.
31. Palani S, Maksimow M, Miiluniemi M, Auvinen K, Jalkanen S, Salmi M. Stabilin-1/CLEVER-1, a type 2 macrophage marker, is an adhesion and scavenging molecule on human placental macrophages. *Eur J Immunol*. 2011;41(7):2052–2063.
32. Martinez FO, et al. Genetic programs expressed in resting and IL-4 alternatively activated mouse and human macrophages: similarities and differences. *Blood*. 2013;121(9):e57–e69.
33. Tsai SY, et al. DAMP molecule S100A9 acts as a molecular pattern to enhance inflammation during influenza A virus infection: role of DDX21-TRIF-TLR4-MyD88 pathway. *PLoS Pathog*. 2014;10(1):e1003848.
34. Xue J, et al. Transcriptome-based network analysis reveals a spectrum model of human macrophage activation. *Immunity*. 2014;40(2):274–288.
35. Mildner A, et al. CCR2+Ly-6Chi monocytes are crucial for the effector phase of autoimmunity in the central nervous system. *Brain*. 2009;132(pt 9):2487–2500.
36. Urban BC, Willcox N, Roberts DJ. A role for CD36 in the regulation of dendritic cell function. *Proc Natl Acad Sci U S A*. 2001;98(15):8750–8755.
37. Kagan JC, Horng T. NLRP3 inflammasome activation: CD36 serves double duty. *Nat Immunol*. 2013;14(8):772–774.
38. Cayrol C, Girard JP. IL-33: an alarmin cytokine with crucial roles in innate immunity, inflammation and allergy. *Curr Opin Immunol*. 2014;31:31–37.
39. Zelenay S, et al. The dendritic cell receptor DNGR-1 controls endocytic handling of necrotic cell antigens to favor cross-priming of CTLs in virus-infected mice. *J Clin Invest*. 2012;122(5):1615–1627.
40. Stocki P, Wang XN, Dickinson AM. Inducible heat shock protein 70 reduces T cell responses and stimulatory capacity of monocyte-derived dendritic cells. *J Biol Chem*. 2012;287(15):12387–12394.
41. Shimizu K, et al. IL-1 receptor type 2 suppresses collagen-induced arthritis by inhibiting IL-1 signal on macrophages. *J Immunol*. 2015;194(7):3156–3168.
42. Torices S, et al. A truncated variant of ASCC1, a novel inhibitor of NF-κB, is associated with disease severity in patients with rheumatoid arthritis. *J Immunol*. 2015;195(11):5415–5420.
43. Pello OM, et al. Role of c-MYC in alternative activation of human macrophages and tumor-associated macrophage biology. *Blood*. 2012;119(2):411–421.
44. Liu L, et al. Proinflammatory signal suppresses proliferation and shifts macrophage metabolism from Myc-dependent to HIF1α-dependent. *Proc Natl Acad Sci U S A*. 2016;113(6):1564–1569.
45. Ugel S, De Sanctis F, Mandruzzato S, Bronte V. Tumor-induced myeloid deviation: when myeloid-derived suppressor cells meet tumor-associated macrophages. *J Clin Invest*. 2015;125(9):3365–3376.
46. Schönheit J, et al. PU.1 level-directed chromatin structure remodeling at the Irf8 gene drives dendritic cell commitment. *Cell Rep*. 2013;3(5):1617–1628.
47. Shih VF, et al. Control of RelB during dendritic cell activation integrates canonical and noncanonical NF-κB pathways. *Nat Immunol*. 2012;13(12):1162–1170.
48. Kanamoto T, Hellman U, Heldin CH, Souchelnytskyi S. Functional proteomics of transforming growth factor-β1-stimulated Mv1Lu epithelial cells: Rad51 as a target of TGFβ1-dependent regulation of DNA repair. *EMBO J*. 2002;21(5):1219–1230.
49. Leikauf GD, et al. Haplotype association mapping of acute lung injury in mice implicates activin a receptor, type 1. *Am J Respir Crit Care Med*. 2011;183(11):1499–1509.
50. Peranzoni E, et al. Role of arginine metabolism in immunity and immunopathology. *Immunobiology*. 2007;212(9-10):795–812.
51. Rani R, Smulian AG, Greaves DR, Hogan SP, Herbert DR. TGF-β limits IL-33 production and promotes the resolution of colitis through regulation of macrophage function. *Eur J Immunol*. 2011;41(7):2000–2009.
52. Ruffell D, et al. A CREB-C/EBPβ cascade induces M2 macrophage-specific gene expression and promotes muscle injury repair. *Proc Natl Acad Sci U S A*. 2009;106(41):17475–17480.
53. Locati M, Mantovani A, Sica A. Macrophage activation and polarization as an adaptive component of innate immunity. *Adv Immunol*. 2013;120:163–184.
54. Biollaz G, et al. Site-specific anti-tumor immunity: differences in DC function, TGF-β production and numbers of intratumoral Foxp3+ Treg. *Eur J Immunol*. 2009;39(5):1323–1333.
55. Arsura M, Wu M, Sonenshein GE. TGF-β1 inhibits NF-κB/Rel activity inducing apoptosis of B cells: transcriptional activation of I kappa Bα. *Immunity*. 1996;5(1):31–40.
56. Ramalingam R, et al. Dendritic cell-specific disruption of TGF-β receptor II leads to altered regulatory T cell phenotype and spontaneous multiorgan autoimmunity. *J Immunol*. 2012;189(8):3878–3893.
57. Robson NC, et al. Activin-A: a novel dendritic

cell-derived cytokine that potently attenuates CD40 ligand-specific cytokine and chemokine production. *Blood*. 2008;111(5):2733–2743.
58. Parsa R, et al. Adoptive transfer of immunomodulatory M2 macrophages prevents type 1 diabetes in NOD mice. *Diabetes*. 2012;61(11):2881–2892.
59. Willems E, et al. Small molecule-mediated TGF-β type II receptor degradation promotes cardiomyogenesis in embryonic stem cells. *Cell Stem Cell*. 2012;11(2):242–252.
60. Levéen P, et al. Induced disruption of the transforming growth factor β type II receptor gene in mice causes a lethal inflammatory disorder that is transplantable. *Blood*. 2002;100(2):560–568.
61. Caton ML, Smith-Raska MR, Reizis B. Notch-RBP-J signaling controls the homeostasis of CD8- dendritic cells in the spleen. *J Exp Med*. 2007;204(7):1653–1664.
62. Sanford LP, et al. TGFβ2 knockout mice have multiple developmental defects that are non-overlapping with other TGFβ knockout phenotypes. *Development*. 1997;124(13):2659–2670.
63. King IL, Dickendesher TL, Segal BM. Circulating Ly-6C+ myeloid precursors migrate to the CNS and play a pathogenic role during autoimmune demyelinating disease. *Blood*. 2009;113(14):3190–3197.
64. Hesske L, et al. Induction of inhibitory central nervous system-derived and stimulatory blood-derived dendritic cells suggests a dual role for granulocyte-macrophage colony-stimulating factor in central nervous system inflammation. *Brain*. 2010;133(pt 6):1637–1654.
65. Fife BT, Huffnagle GB, Kuziel WA, Karpus WJ. CC chemokine receptor 2 is critical for induction of experimental autoimmune encephalomyelitis. *J Exp Med*. 2000;192(6):899–905.
66. Ajami B, Bennett JL, Krieger C, McNagny KM, Rossi FM. Infiltrating monocytes trigger EAE progression, but do not contribute to the resident microglia pool. *Nat Neurosci*. 2011;14(9):1142–1149.
67. McQualter JL, et al. Granulocyte macrophage colony-stimulating factor: a new putative therapeutic target in multiple sclerosis. *J Exp Med*. 2001;194(7):873–882.
68. Ponomarev ED, Shriver LP, Maresz K, Pedras-Vasconcelos J, Verthelyi D, Dittel BN. GM-CSF production by autoreactive T cells is required for the activation of microglial cells and the onset of experimental autoimmune encephalomyelitis. *J Immunol*. 2007;178(1):39–48.
69. Campbell IK, Rich MJ, Bischof RJ, Dunn AR, Grail D, Hamilton JA. Protection from collagen-induced arthritis in granulocyte-macrophage colony-stimulating factor-deficient mice. *J Immunol*. 1998;161(7):3639–3644.
70. Sonderegger I, Iezzi G, Maier R, Schmitz N, Kurrer M, Kopf M. GM-CSF mediates autoimmunity by enhancing IL-6-dependent Th17 cell development and survival. *J Exp Med*. 2008;205(10):2281–2294.
71. Langrish CL, et al. IL-23 drives a pathogenic T cell population that induces autoimmune inflammation. *J Exp Med*. 2005;201(2):233–240.
72. McGeachy MJ, et al. The interleukin 23 receptor is essential for the terminal differentiation of interleukin 17-producing effector T helper cells in vivo. *Nat Immunol*. 2009;10(3):314–324.
73. Jain R, et al. Interleukin-23-induced transcription factor Blimp-1 promotes pathogenicity of T helper 17 cells. *Immunity*. 2016;44(1):131–142.
74. Kara EE, et al. CCR2 defines in vivo development and homing of IL-23-driven GM-CSF-producing Th17 cells. *Nat Commun*. 2015;6:8644.
75. Gaublomme JT, et al. Single-cell genomics unveils critical regulators of Th17 cell pathogenicity. *Cell*. 2015;163(6):1400–1412.
76. Nairz M, et al. Nitric oxide-mediated regulation of ferroportin-1 controls macrophage iron homeostasis and immune function in Salmonella infection. *J Exp Med*. 2013;210(5):855–873.
77. Aliper AM, Frieden-Korovkina VP, Buzdin A, Roumiantsev SA, Zhavoronkov A. Interactome analysis of myeloid-derived suppressor cells in murine models of colon and breast cancer. *Oncotarget*. 2014;5(22):11345–11353.
78. Papaspyridonos M, et al. Id1 suppresses anti-tumour immune responses and promotes tumour progression by impairing myeloid cell maturation. *Nat Commun*. 2015;6:6840.
79. Qian BZ, Pollard JW. Macrophage diversity enhances tumor progression and metastasis. *Cell*. 2010;141(1):39–51.
80. Balkwill F. Cancer and the chemokine network. *Nat Rev Cancer*. 2004;4(7):540–550.
81. Ramalingam R, et al. Dendritic cell-specific disruption of TGF-β receptor II leads to altered regulatory T cell phenotype and spontaneous multiorgan autoimmunity. *J Immunol*. 2012;189(8):3878–3893.
82. Laouar Y, et al. TGF-β signaling in dendritic cells is a prerequisite for the control of autoimmune encephalomyelitis. *Proc Natl Acad Sci U S A*. 2008;105(31):10865–10870.
83. Speck S, et al. TGF-β signaling initiated in dendritic cells instructs suppressive effects on Th17 differentiation at the site of neuroinflammation. *PLoS One*. 2014;9(7):e102390.
84. Fabry Z, et al. TGF-β2 decreases migration of lymphocytes in vitro and homing of cells into the central nervous system in vivo. *J Immunol*. 1995;155(1):325–332.
85. Siglienti I, et al. Downregulation of transforming growth factor-beta2 facilitates inflammation in the central nervous system by reciprocal astrocyte/microglia interactions. *J Neuropathol Exp Neurol*. 2007;66(1):47–56.
86. Drescher KM, Murray PD, Lin X, Carlino JA, Rodriguez M. TGF-β2 reduces demyelination, virus antigen expression, and macrophage recruitment in a viral model of multiple sclerosis. *J Immunol*. 2000;164(6):3207–3213.
87. Parsa R, et al. TGFβ regulates persistent neuroinflammation by controlling Th1 polarization and ROS production via monocyte-derived dendritic cells. *Glia*. 2016;64(11):1925–1937.
88. Hucke S, et al. The farnesoid-X-receptor in myeloid cells controls CNS autoimmunity in an IL-10-dependent fashion. *Acta Neuropathol*. 2016;132(3):413–431.
89. Bettelli E, Pagany M, Weiner HL, Linington C, Sobel RA, Kuchroo VK. Myelin oligodendrocyte glycoprotein-specific T cell receptor transgenic mice develop spontaneous autoimmune optic neuritis. *J Exp Med*. 2003;197(9):1073–1081.
90. Tropepe V, Sibilia M, Ciruna BG, Rossant J, Wagner EF, van der Kooy D. Distinct neural stem cells proliferate in response to EGF and FGF in the developing mouse telencephalon. *Dev Biol*. 1999;208(1):166–188.
91. Pluchino S, et al. Immune regulatory neural stem/precursor cells protect from central nervous system autoimmunity by restraining dendritic cell function. *PLoS One*. 2009;4(6):e5959.
92. Rovere-Querini P, et al. HMGB1 is an endogenous immune adjuvant released by necrotic cells. *EMBO Rep*. 2004;5(8):825–830.
93. Ginhoux F, et al. Fate mapping analysis reveals that adult microglia derive from primitive macrophages. *Science*. 2010;330(6005):841–845.